nature communications

Article

https://doi.org/10.1038/s41467-025-57980-7

Global characterization of mouse testis O-glycoproteome landscape during spermatogenesis

Received: 13 May 2024

Accepted: 7 March 2025

Published online: 18 March 2025

Check for updates

Qiannan Liu[1,5], Xiaoyan Lu[1,5], Yao Deng[1], Han Zhang[1], Rumeng Wei[1], Hongrui Li[1], Ying Feng[2], Juan Wei[3], Fang Ma[4], Yan Zhang[1] ✉ & Xia Zou[1] ✉

Protein O-glycosylation plays critical roles in sperm formation and maturation. However, detailed knowledge on the mechanisms involved is limited due to lacking characterization of O-glycoproteome of testicular germ cells. Here, we performed a systematic analysis of site-specific O-glycosylation in mouse testis, and established an O-glycoproteome map with 349 O-glycoproteins and 799 unambiguous O-glycosites. Moreover, we comprehensively investigated the distribution properties of O-glycosylation in testis and identified a region near the N-terminal of peptidase S1 domain that is susceptible to O-glycosylation. Interestingly, we found dynamic changes with an increase Tn and a decrease T structure from early to mature developmental stages. Notably, the importance of O-glycosylation was supported by its effects on the stability, cleavage, and interaction of acrosomal proteins. Collectively, these data illustrate the global properties of O-glycosylation in testis, providing insights and resources for future functional studies targeting O-glycosylation dysregulation in male infertility.

Infertility has emerged as a global health problem and is estimated to affect 10–20% of couples of reproductive age worldwide[1]. In China, over 40 million people suffer from infertility, and this number is still showing a rapid increasing trend[2]. Of all the infertility cases, approximately 50% are due to males. Congenital or acquired factors that impair or affect spermatogenesis are major causes of male infertility[3].

Spermatogenesis is a highly complex process that occurs in the seminiferous tubules of testis. The spermatogonia undergo mitosis and meiosis to form spermatocytes, round spermatids, and eventually elongated spermatids which are then released into the lumen of the seminiferous tubules[4]. The surface of mammalian sperm is coated with a 20–60 nm thick glycocalyx containing abundant N-glycoproteins, O-glycoproteins, glycolipids and so on[5]. It is becoming increasingly evident that sperm glycosylation plays essential roles in the entire process of spermatogenesis, maturation, capacitation, sperm-egg recognition, and fertilization. Over the past two decades, due to the rapid development of mass spectrometry (MS)-based technologies, considerable progress has been made in in-depth characterization of N-glycoproteins in sperm. Increasing glycomic and glycoproteomic studies have delineated a clearer picture of the composition of N-glycoproteins, N-glycosylation sites, and N-glycan structures in spermatozoa[6,7], epididymal sperm[8], and seminal plasma[9–11]. These glycomic knowledge further contribute to our understanding of the roles of N-glycans in spermatogenesis. For example, MS analysis showed that the majority of N-glycan structures in seminal plasma was complex type[10,11]. Functional studies confirmed that the loss of complex N-glycans caused a block in spermatogenesis by promoting the premature upregulation of genes normally expressed during late stages of spermatogenesis[12]. However, compared with many studies in N-glycosylation, there are still less studies on O-glycosylation in sperm.

[1]Key Laboratory of Systems Biomedicine (Ministry of Education), Shanghai Center for Systems Biomedicine, Center for Chemical Glycobiology, Zhang Jiang Institute for Advanced Study, Shanghai Jiao Tong University, Shanghai, China. [2]West China School of Basic Medical Sciences & Forensic Medicine, Sichuan University, Chengdu, Sichuan, China. [3]School of Pharmacy, Shanghai Jiao Tong University, Shanghai, China. [4]Center for Translational Medicine, Key Laboratory of Birth Defects and Related Diseases of Women and Children (Sichuan University), Ministry of Education, West China Second University Hospital, Sichuan University, Chengdu, Sichuan, China. [5]These authors contributed equally: Qiannan Liu, Xiaoyan Lu. ✉e-mail: yanzhang2006@sjtu.edu.cn; zouxia0206@sjtu.edu.cn

O-glycosylation is one of the most common and diverse types of glycosylation, which primarily occurs at serine (Ser) or threonine (Thr). Based on the differences in the first monosaccharide linked to amino acids, O-glycosylation can be divided into many forms. O-GalNAc glycosylation (also known as mucin type O-glycosylation) is the most abundant and diverse type of O-glycosylation, playing essential roles in many physiological and pathological processes such as cell differentiation, tissue development, immune recognition, and viral infection[13,14]. O-GalNAc glycosylation is initiated by the polypeptide N-acetyl-α-galactosaminyltransferase family (ppGalNAc-Ts) comprising 20 isoenzymes in human, which transfer GalNAc monosaccharide onto Ser/Thr residues resulting in the formation of Tn antigen (GalNAc-α1-Ser/Thr)[14,15]. The initiating Tn structure can be subsequently extended to form the most common core 1 structure (T antigen, Galβ1,3GalNAc-α1-Ser/Thr)[16], or other common core structures, which can be further elongated or branched in a stepwise manner (Fig. 1a)[14,15].

In our previous work, we developed a lectin microarray-based method to detect the glycome profile in different organs of adult mice, and surprisingly found that testis had the highest level of O-GalNAc glycosylation compared with brain, liver, spleen, and kidney[17]. The high level of O-GalNAc glycans in spermatozoa was also verified by O-glycan antibodies[18]. Additionally, studies on specific proteins have shown the importance of O-GalNAc glycosylation in sperm development. For example, Franke et al. found a significant difference in the O-GalNAc glycosylation pattern of mucin 1 (MUC1) between testes with normal and impaired spermatogenesis. Notably, two members of ppGalNAc-Ts family, ppGalNAc-T3 (GALNT3) and T19 (GALNTL5) were highly expressed in spermatocytes and/or spermatids in the testis, and knockout mice for both genes were sterile[19,20]. In detail, the deficiency of *Galnt3* resulted in a severe reduction of mucin-type O-glycans in spermatids and caused impaired acrosome formation, leading to oligoasthenoteratozoospermia[19]. In human semen samples, ppGalNAc-T3 and the O-glycans Tn and T were found in spermatozoa, with a positive correlation observed between the expression of ppGalNAc-T3 and classical semen parameters[21]. The mutation of *Galntl5* attenuated glycolytic enzymes required for motility, disrupted the localization of ubiquitin–proteasome system, leading to asthenozoospermia[20]. Moreover, the lectins *Agaricus bisporus* agglutinin (ABA) and *Maclura pomifera* lectin (MPL), which recognize O-GalNAc glycans, have been reported as potential biomarkers for the diagnosis of male subfertility caused by *DEFB126* deficiency[22]. Overall, these studies indicate that O-GalNAc glycosylation (hereinafter referred to as O-glycosylation) in the testis plays an essential role in spermatogenesis and is closely related to infertility. To deeply investigate the functional mechanisms involved, the first key questions to be addressed are: which proteins are O-glycosylated, what are the location and structure of O-glycans on them, and how do they change during spermatogenesis. However, the characterization of the O-glycoproteome has lagged behind due to the lack of conserved amino acid sequences at O-glycosites as well as the complexity and heterogeneity of O-glycan structures. To the best of our knowledge, no systematic O-glycoproteomics studies of the testis have been performed to date.

Here, we present a large-scale site-specific O-glycoproteome study to characterize protein O-glycosylation in the testis during spermatogenesis. We first detect the modification pattern of O-glycan in the testis at different stages of spermatogenesis by lectin staining. Our findings highlight prominent O-glycan levels in round and elongated spermatids, but not in spermatogonia or spermatocytes. Subsequently, using lectin affinity enrichment coupled with liquid chromatography-tandem mass spectrometry (LC-MS/MS), we further perform a systematic qualitative and quantitative analysis of the O-glycoproteome in 24-day-old and 12-week-old testes, elucidate the distribution properties of O-glycoproteins and O-glycosites, and discover the dynamic level of O-glycosylation with increased Tn structure and decreased T structure in mature testes. Finally, we preliminarily explore the possible functions of O-glycosylation in highly O-glycosylated proteins related to fertilization, and verify the regulatory roles of GALNT3, providing resources for future functional studies targeting O-glycosylation in spermatogenesis and fertilization.

Results

O-glycans are located in round and elongated spermatids

In this study, we first analyzed the glycome profile data from 14 tissues in a public database[23] and reconfirmed that the testis is an organ exhibiting a high level of O-glycans (Supplementary Fig. 1). To investigate the detailed location of O-glycans in different testicular germ cells, we performed lectin staining of testicular tissues at six time points according to the developmental timeline of mouse germ cell (Fig. 1b)[24–26]. At 0 and 7 days after birth, only spermatogonia are present. At 16 days postpartum, spermatocytes are dominant cell type. At 24 days postpartum, elongated spermatids are not yet appeared, while round spermatids account for a higher proportion of germ cells compared to earlier stages, despite spermatocytes remaining a predominant cell type. At 8 and 12 weeks postpartum, elongated spermatids become the most abundant type of germ cells in seminiferous tubules. Two lectins, namely *vicia villosa agglutinin* (VVA) and *peanut* agglutinin (PNA), were used to detect the main types of O-glycan in the testis. The VVA lectin is a family of tetrameric proteins consisting of combinations of A and B subunits[27]. The isolectin used in this study is primarily composed of the B subunit, which is also the predominant subtype of VVA lectin and has been widely reported to recognize terminal α-linked GalNAc residues (Tn antigen)[28,29]. In contrast, the PNA lectin has been demonstrated to exhibit the strongest specificity for the disaccharide Galβ1→3GalNAc (T antigen)[30] (Fig. 1a).

As shown in Fig. 1c, both signals of PNA and VVA appeared only after 24 days postnatal, indicating that O-glycans in the testis are mainly located in round and elongated spermatids, whereas they are barely present in spermatogonia or spermatocytes. Notably, the signals of O-glycans were strongest in the acrosome of the spermatid heads. In addition, we found that spermatids have preferences for different O-glycans. That is, the signals of T structure recognized by PNA were stronger in round spermatids (hollow arrowheads), whereas the signals of Tn structure recognized by VVA were stronger in elongated spermatids (solid arrowheads), suggesting that O-glycans may be involved in the spermatozoa formation and maturation.

Global characterization of O-glycoproteome in mouse testes

To identify proteins undergoing O-glycosylated during spermiogenesis, we analyzed the global O-glycoproteome using testes of 24-day-old mice characterized by a higher proportion of round spermatids compared to earlier stages, and 12-week-old mice characterized by elongated spermatids being the predominant germ cells within the seminiferous tubules. As shown in Fig. 2a, de-sialylated peptides from testes were enriched by VVA and PNA lectins respectively. O-glycopeptides were then identified by mass spectrometry using higher-energy dissociation product ions-triggered electron-transfer/higher-energy collision dissociation (HCD-pd-EThcD) strategy and analyzed with pGlyco3[31] and MetaMorpheus[32]. All the spectrum were checked by HexNAcQuest[33] to exclude O-GlcNAc glycopeptides. As a result, a total of 349 O-GalNAc glycoproteins (Supplementary Data 1) with 16,227 glycopeptide-spectrum matches (GPSM) were detected. On these glycoproteins, there were 647 unique O-glycopeptides containing 799 unambiguous O-glycosites (Fig. 2b, c). Notably, more O-glycoproteins were found in the testes of 24-day-old mice (307/349), especially within the PNA-enriched group, reflecting active O-glycoprotein biosynthesis in round spermatids when the Golgi synthesizes large amounts of glycoproteins and delivers them to the acrosome[34].

Comparison with the recently reported atlas of mouse O-glycoproteins summarized by Yang et al.[35], we identified an

https://doi.org/10.1038/s41467-025-57980-7

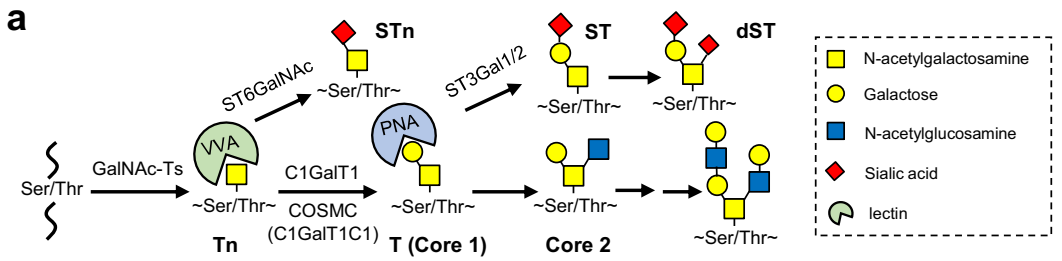

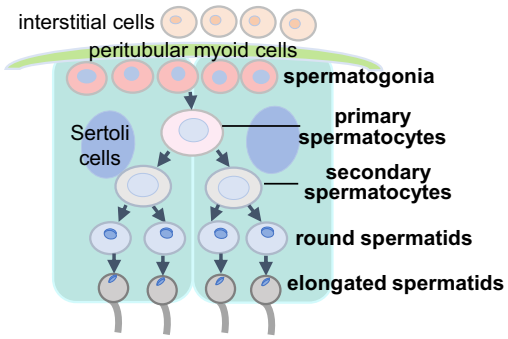

Post-partum	Germ cell types
0, 7 days	only spermatogonia
16 days	spermatogonia and more primary spermatocytes
24 days	spermatogonia, spermatocytes and round spermatids
over 8 weeks	all types; elongated spermatids are the most abundant cell type

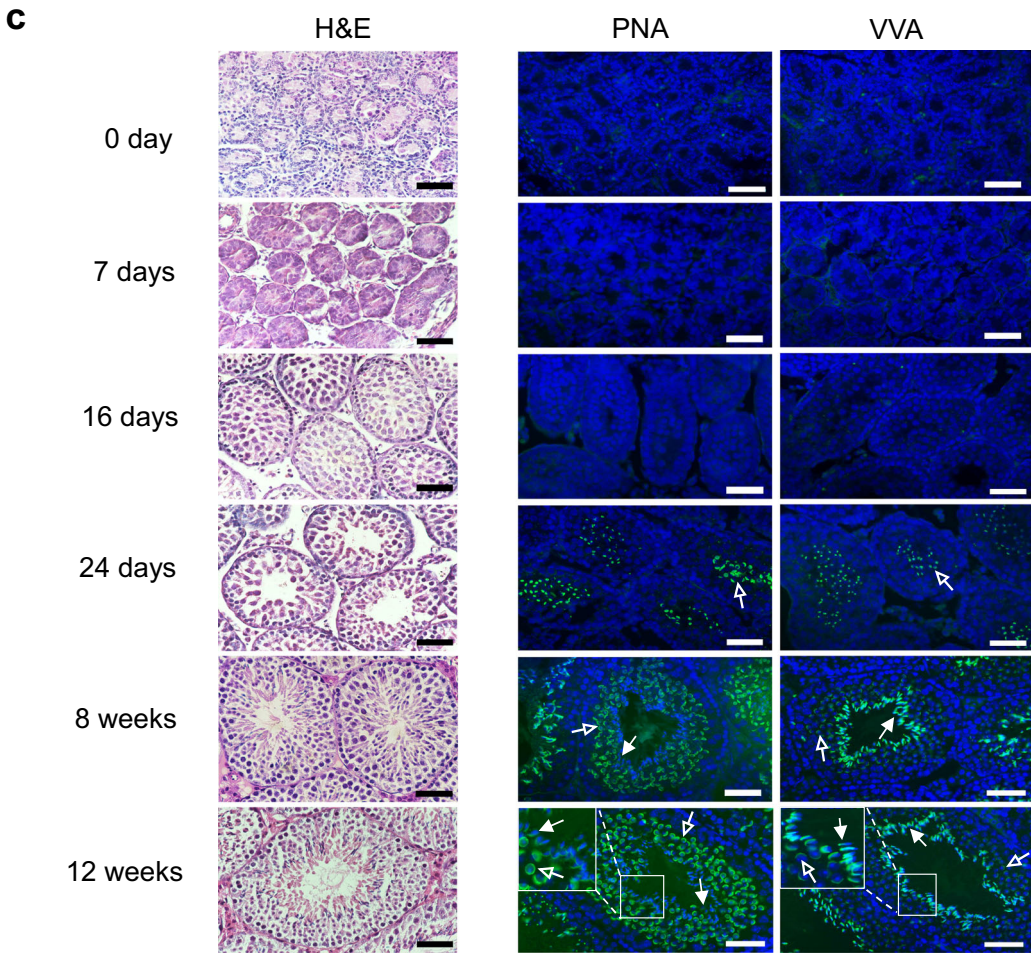

Fig. 1 | Cellular localization of O-GalNAc glycans in mouse testes at different ages. a Illustration of the major O-GalNAc glycans. Biosynthesis and extension of Tn and T structures were shown. **b** Schematic diagram of different stages of spermatogenesis. The spermatogonia perform a mitotic division to form primary spermatocytes. The latter undergo two meiotic divisions to form round spermatids, which subsequently undergo a structural metamorphosis to become elongated spermatids. The composition of germ cell types in seminiferous tubules of mouse testes from 0 day after birth until sexual maturity was summarized according to literature. **c** H&E (Hematoxylin and Eosin) staining (left) and lectin staining (middle and right) of seminiferous tubules of mouse testes at different times after birth. The signal of PNA (*peanut* agglutinin) recognizing T antigen (Galβ1,3GalNAc-α1-Ser/Thr) was strongly stained in round and elongated spermatids, especially in round spermatids. The signal of VVA (*vicia villosa* agglutinin) recognizing Tn antigen (GalNAc-α1-Ser/Thr) was strongly stained in round and elongated spermatids, especially in elongated ones. White hollow and solid arrows indicate round and elongated spermatids, respectively. The images shown are representative of five mice/group. Scale bars represent 50 μm. STn sialylated Tn antigen, ST sialylated T antigen, dST di-sialylated T antigen.

https://doi.org/10.1038/s41467-025-57980-7

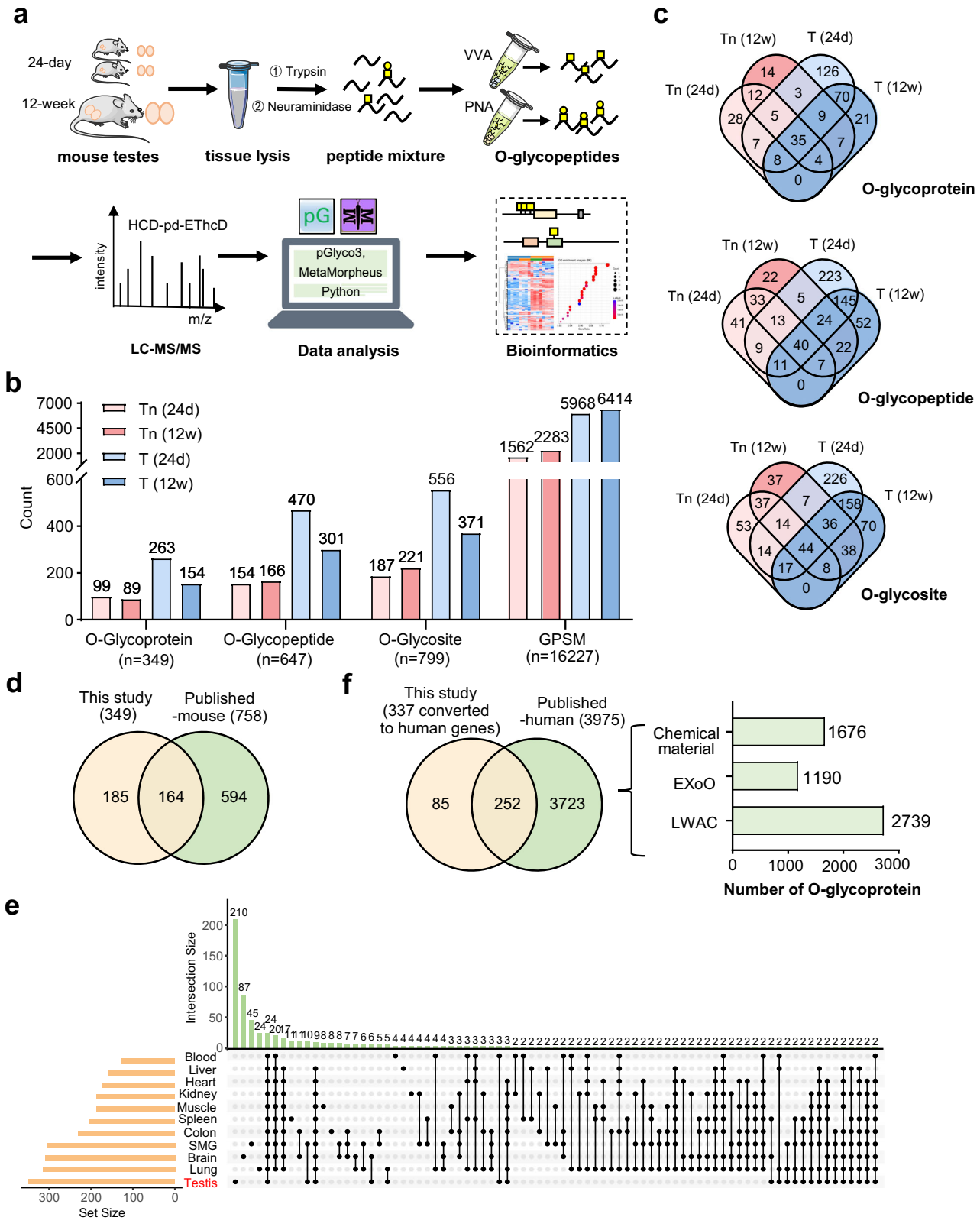

additional 185 mouse O-glycoproteins (Fig. 2d). In particular, when compared with the O-glycoproteins of the other 10 mouse organs in that report[35], we found that the testis had the most abundant and specific O-glycoproteins (Fig. 2e). Moreover, since O-glycoproteomic research in humans is much more advanced, we summarized 3975 published human O-glycoproteins identified by lectin weak affinity chromatography (LWAC) enrichment strategy[36–50], chemical material enrichment strategy[51–58], and extraction of O-linked glycopeptides (EXoO) using OpeRATOR protease[59,60] (Fig. 2f). We converted the mouse glycoproteins identified in this study to human homologs and discovered 85 additional glycoproteins not reported in the human O-GalNAc glycoprotein database (Fig. 2f and Supplementary Data 1).

Fig. 2 | In-depth characterization of the O-glycoproteome in testes of 24-day-old and 12-week-old mice. a Schematic workflow for analyzing the testis O-glycoproteome. Proteins from testes of 24-day-old and 12-week-old mice were extracted, digested by trypsin, and subsequently de-sialylated using neuraminidase. The O-glycopeptides with Tn and T structures were enriched using VVA and PNA lectins respectively, and then identified by LC-MS/MS using higher-energy dissociation product ions-triggered electron-transfer/higher-energy collision dissociation (HCD-pd-EThcD) strategy. Four biological replicates were used for each group. Illustrations used elements from Servier Medical Art (http://smart.servier.com/) under a Creative Common Attribution 3.0 Generic License (https://creativecommons.org/licenses/by/3.0/). **b** The numbers of O-glycoproteins, unique O-glycopeptides, unambiguous O-glycosites, and glycopeptide-spectrum matches (GPSM) identified in each group. **c** Venn diagram showing the distribution of identified O-glycoproteins, O-glycopeptides, and O-glycosites enriched from testes at different developmental stages using different lectins. **d**, **e** Overlap of the testis O-glycoproteins identified in this study with those from the previously reported mouse O-glycoproteins atlas (**d**), as well as with the reported O-glycoproteins of the other 10 mouse organs published by Yang et al.[35]. (**e**, **f**) Overlap of human counterparts of the 337 mouse O-glycoproteins with the published human O-glycoproteins which were mainly identified by chemical methods, LWAC or EXoO strategy. VVA *vicia villosa* agglutinin, PNA *peanut* agglutinin, Tn GalNAc-α1-Ser/Thr, T Galβ1,3GalNAc-α1-Ser/Thr, GPSM glycopeptide-spectrum matches, LWAC lectin weak affinity chromatography, EXoO site-specific extraction of O-linked glycopeptides.

Distribution characteristics of O-glycosites in mouse testes

Since the density and location of the O-glycosites on proteins are closely related to the potential functions of O-glycans[36,38,42,48], we next sought to map these characteristics of the O-glycosites identified in mouse testes. First, we performed overall statistical analyses on O-glycosites. As a result, 69.6% of the O-glycopeptides and 56% of the O-glycoproteins identified in the present study carried ≤ 2 unambiguous O-glycosites, whereas 20 peptides (3.1%) and 11 proteins (3.2%) were found to be highly glycosylated, carrying ≥ 5 sites and ≥10 sites, respectively (Fig. 3a, b). Notably, many of these highly O-glycosylated proteins have been reported to be directly involved in spermatogenesis and fertilization, such as acrosin-binding protein (ACRBP), equatorial segment protein 1 (SPESP1), and sperm acrosome-associated protein 7 (SPACA7), which not only have a large number of glycosylation sites but also high coverage of glycopeptides (≥5) and high abundance of GPSM (>100) (Fig. 3c). Intriguingly, statistics of GPSM for the 20 O-glycopeptides with dense glycosylation (≥5 sites) showed that almost all glycopeptides specifically or highly expressed in testes had the highest GPSM counts in 12-week-old testes (Fig. 3d), suggesting that the degree of O-glycosylation in mature spermatozoa is higher than that in round spermatozoa.

Next, we further analyzed the distribution pattern of the 799 unambiguous O-glycosites in protein structural domains annotated in the UniProt database. We found that only 7.5% (60 sites) were located within specific domains and tended to be localized on both sides rather than in the middle of the domains, which was particularly evident in domains of LDL receptor class A, Ig-like C2-type, fibronectin type III, and EF-hand (Supplementary Fig. 2a). In contrast, up to 19.4% (155 sites) were located within 20 amino acids of the N- or C-terminal of the domains. It was observed that many O-glycosites were distributed at the outer edges rather than the inner edges of the domains (Fig. 3e). Additionally, using the mouse proteome database consisting of 17,228 proteins (UniProtKB reviewed, Swiss-Prot) as a background, we found that proteins containing O-glycosites near cleavage sites, stem regions (within 50 amino acids from transmembrane domain), and ER retention motifs (KDEL and similar sequences), as well as on precursor peptides, were almost significantly enriched in the testis ($p < 0.05$) (Supplementary Fig. 2b and Supplementary Data 2). This result is in accordance with previous reports using other biological models[36,42]. Notably, apart from these findings, we identified a region near the N-terminal of peptidase S1 domain which is susceptible to O-glycosylation (Fig. 3f, g). The dense O-glycosites around the peptidase S1 domain on different members of this protease family (PRSS40, 42, 43, 44, 50) suggest that O-glycosylation may play a significant role in the maturation and shearing of proteins during spermatogenesis.

Overall, among the 799 unambiguous O-glycosites identified in testes, 37.5% (300 sites) were distributed in disordered regions, and 19.4% (155 sites) were located within 20 amino acids of the N- or C-terminal edges of specific protein structural domains. Additionally, 11.0% (88 sites) were localized to the stem regions of transmembrane proteins, suggesting the role of O-glycans in maintaining structural stability[48]. Another 10.9% (87 sites) were located in specific functional regions related to protein interactions, folding and trafficking, indicating the potential effect of site-specific O-glycosylation on protein functions. Taken together, we systematically mapped the association between identified O-glycosites and their location on proteins, providing important clues for understanding the biological functions of site-specific O-glycosylation in spermatids.

Differential O-glycopeptides involve in spermatogenesis and fertilization

After mapping the O-glycoproteins and O-glycosites in the testis, we performed label-free quantitative analysis of the O-glycopeptides. Correlation analysis revealed a high correlation among the four biological replicates within the same group ($r^2 > 0.85$), suggesting good repeatability and reliable quantification (Supplementary Fig. 3a). Principal component analysis (PCA) demonstrated that intact O-glycopeptides enriched at different developmental stages using distinct lectins were clearly separated (Supplementary Fig. 3b). Hierarchical clustering analysis further showed that overall glycopeptide intensity was higher in 12-week-old testes than in 24-day-old testes in the VVA-enriched subset, whereas it was opposite in the PNA-enriched subset (Fig. 4a). Moreover, it was observed that in 24-day-old testes, the H1N1 glycoform accounted for 57.2% (2668) of total GPSM, and the N1 glycoform represented 21.2% (989). In contrast, in 12-week-old samples, the proportions of H1N1 and N1 glycoform were 47.4% (2847) and 27.4% (1647), respectively, indicating an increase in Tn structure and a decrease in T structure in 12-week-old testes with more mature elongated spermatids (Fig. 4b).

After the exclusion of glycopeptides identified in fewer than two biological replicates in at least one group, a $p < 0.05$ and a $|\text{fold change}| > 2$ were set as thresholds for differential glycopeptides. As a result, 63 up-regulated and eight down-regulated O-glycopeptides in the VVA-enriched subset, and 56 up-regulated and 126 down-regulated O-glycopeptides in the PNA-enriched subset, were identified (Fig. 4c, d, and Supplementary Data 3). Considering that changes in O-glycopeptide abundance might result from either altered O-glycosylation levels or altered protein expression, we analyzed reported protein expression levels from round to elongated spermatids[61,62]. However, only 74 of the 232 differential glycopeptides had corresponding protein abundance data. Among these, 59 (79%) glycopeptides exhibited glycosylation alterations that were at least two-fold greater than protein expression alterations, indicating that the observed changes in these O-glycopeptide abundance were primarily due to altered levels of O-glycans (Supplementary Fig. 4 and Supplementary Data 3). For example, the protein level of CD55 did not change significantly, but the glycoforms at all four O-glycosites on the identified glycopeptide were transitioned from T structure in 24-day-old testes to Tn structures in 12-week-old testes (Supplementary Fig. 5a, b). Additionally, 15 (21%) glycopeptides whose changes in abundance may be due to altered protein expression, such as vitronectin (VTN), were also observed (Supplementary Fig. 5c, d).

Further Gene Ontology (GO) analysis showed that the up-regulated O-glycoproteins in the 12-week-old testes were primarily concentrated in the acrosome and spermatid tail, and mainly

https://doi.org/10.1038/s41467-025-57980-7

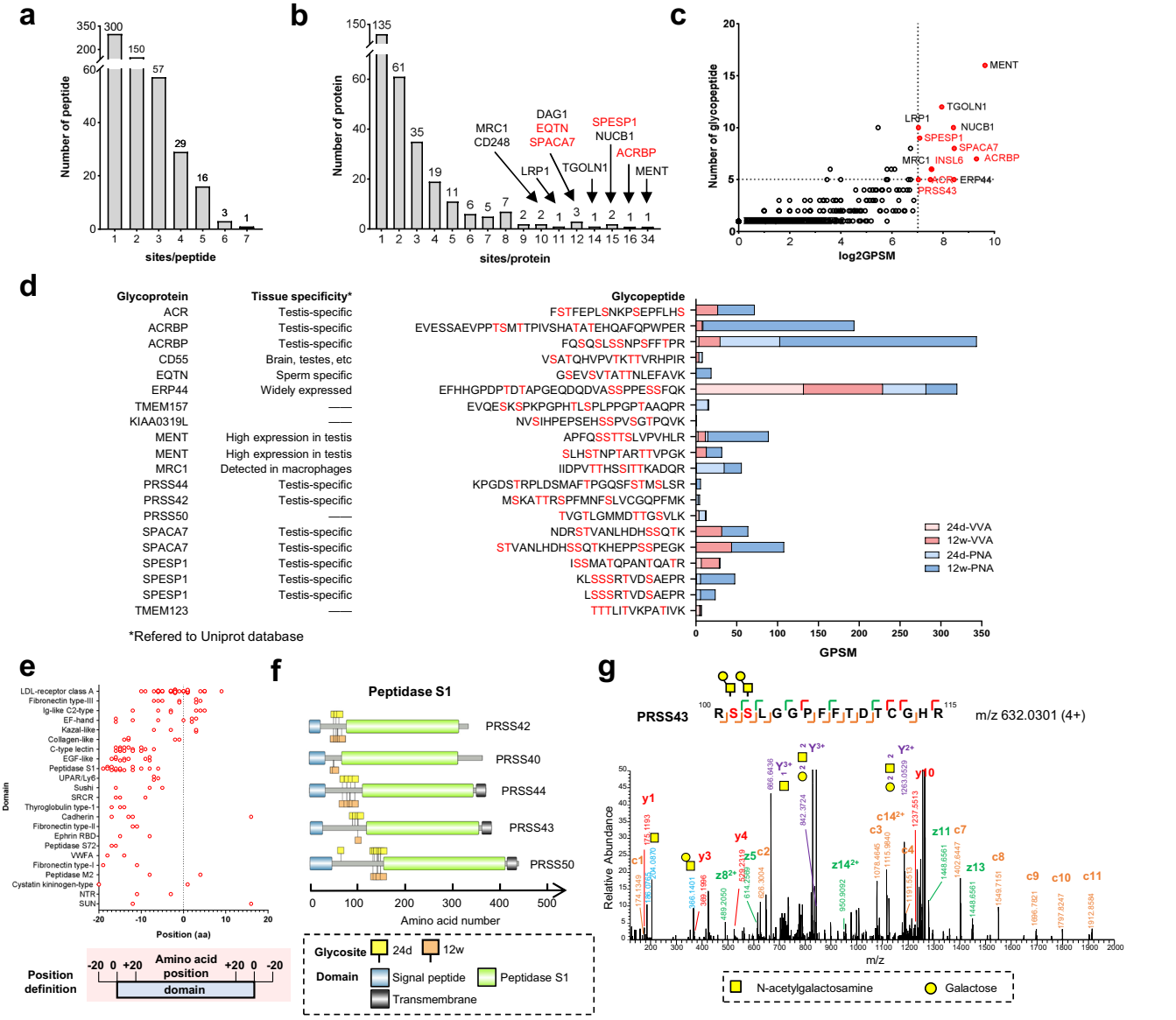

Fig. 3 | Density mapping and distribution preference of O-glycosites in mouse testes. a, **b** The number of unambiguous O-glycosites per peptide (**a**) and per protein (**b**). Glycoproteins involved in spermatogenesis and fertilization were labeled red. **c** The number of unique O-glycopeptides and GPSM per protein. The glycoproteins with a high number of glycopeptides (≥ 5) and high abundance of GPSM (> 100) were labeled in red. **d** Twenty glycopeptides with dense O-glycosites (≥ 5) were listed, and the tissue specificity of the corresponding proteins was shown with reference to the UniProt database. The histogram shows the number of GPSM of these glycopeptides identified in each group. **e** The protein domains containing O-glycosites located at the outer or inner edges (≥ 2 sites) were shown. The domain edge is defined as 20 amino acids located inside (inner edge, positive) or outside (outer edge, negative) the N-/C-terminal of the domain. **f** A region near the N-terminal of domain peptidase S1 domain was found to be susceptible to O-glycosylation. The glycosites identified in testes of 24-day-old and 12-week-old mice are indicated by yellow and orange boxes, respectively. **g** An illustrative annotated MS2 spectrum of the O-glycopeptide from PRSS43 modified with T structure [Hex(1)HexNAc(1)] was shown. **h** Summary of distribution percentage of 799 O-glycosites identified in mouse testes. Protein annotations were referred against the UniProt database. GPSM glycopeptide-spectrum matches, VVA *vicia villosa* agglutinin, PNA *peanut* agglutinin. Source data are provided as a Source Data file.

https://doi.org/10.1038/s41467-025-57980-7

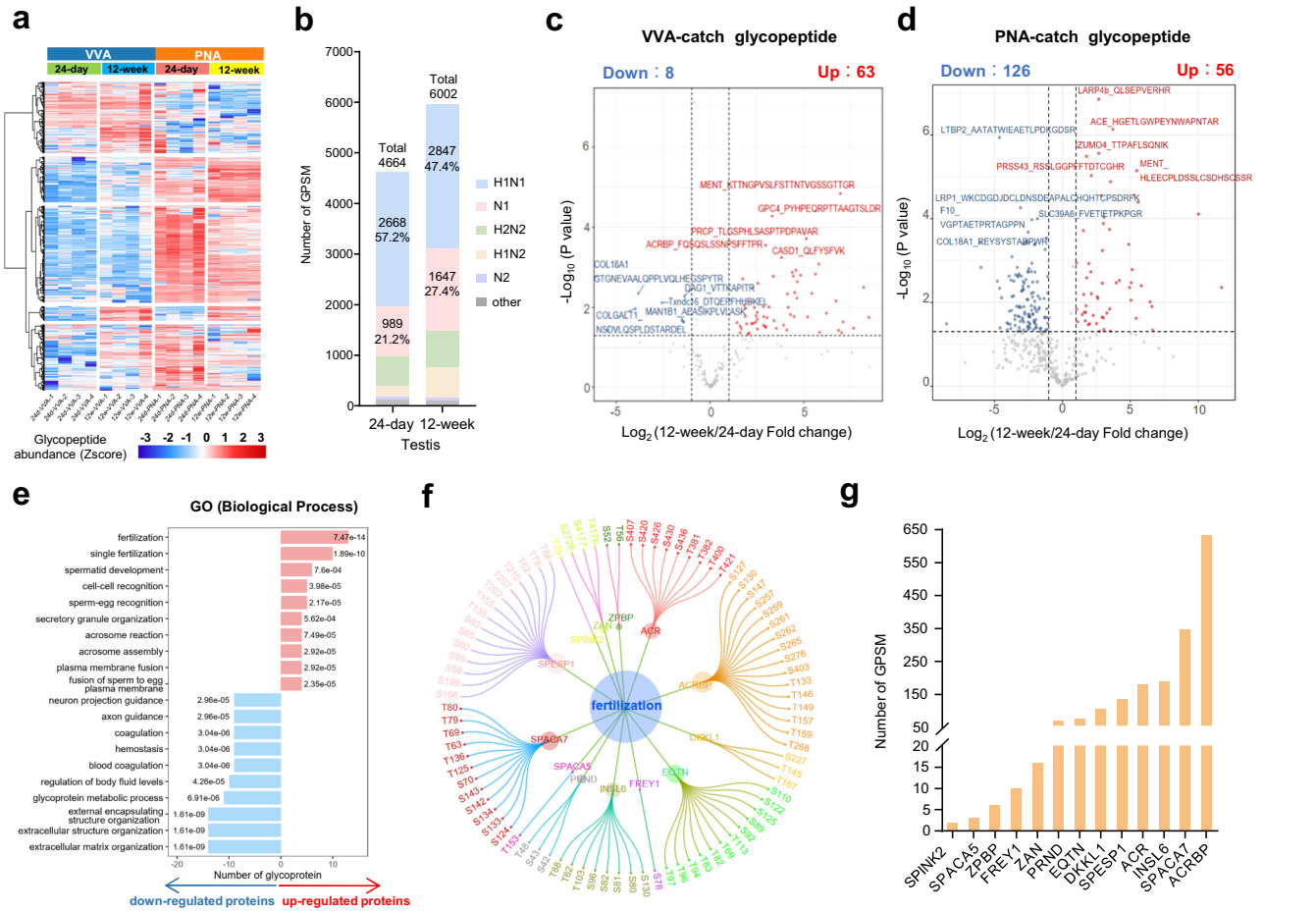

Fig. 4 | Quantitative analysis of O-glycopeptides identified in mouse testes at different stages of spermatogenesis. a Unsupervised hierarchical clustering analysis of O-glycopeptides enriched with VVA or PNA lectin from 24-day-old and 12-week-old testes. The label-free quantitative data of O-glycopeptides were obtained using pGlycoQuant. **b** The distribution of glycan compositions on unambiguous O-glycosites identified in 24-day-old and 12-week-old testes. The number and percentage of GPSM corresponding to H1N1 and N1 glycans were shown. **c**, **d** Volcano plots of individual O-glycopeptide abundance fold changes (log2 scale) and corresponding *p*-values (-log10 scale) enriched by VVA (**c**) or PNA (**d**). The p-value was calculated by two-tailed Student's *t*-test. Up-regulated and down-regulated glycopeptides (with > 2-fold changes and $p < 0.05$) were highlighted in red and blue, respectively, and the top 10 glycopeptides in each group having the lowest p-values were labeled. **e** Gene Ontology (GO) biological process terms enriched in up-regulated and down-regulated glycoproteins in testes of 12-week-old mice. Significance was calculated by one-tailed Fisher's Exact Test (Benjamini-Hochberg FDR-adjusted $p < 0.05$). The top 10 up-regulated (red) and down-regulated (blue) terms with the lowest p-values were shown. **f**, **g** Differential glycoproteins involving in fertilization were depicted. The unambiguous O-glycosites (**f**) and the number of GPSM (**g**) of the 13 glycoproteins with altered abundance between testes of 24-day-old and 12-week-old mice were shown. VVA *vicia villosa* agglutinin, PNA *peanut* agglutinin, H Hexose, N N-acetylhexosamine, GPSM glycopeptide-spectrum matches. Source data are provided as a Source Data file.

involved in spermatogenesis and fertilization processes, whereas the down-regulated proteins were predominantly located in membrane, lipid, and extracellular regions, and most significantly enriched in extracellular structure organization (Fig. 4e and Supplementary Fig. 6a). This observation may be related to the maturation and release process of elongated spermatids. Moreover, we focused on O-glycoproteins associated with spermatogenesis and fertilization, mapping the landscape of their O-glycosites (Fig. 4f) and GPSM (Fig. 4g). Notably, ACRBP, acrosin (ACR), SPACA7, SPESP1, insulin-like peptide 6 (INSL6), and equatorin (EQTN) exhibted the highest number of O-glycosites and GPSM, implying that O-glycosylation may affect spermatogenesis and fertilization through these proteins.

Different O-glycosylation patterns between round and elongated spermatids

After comprehensively analyzing the O-glycoproteome in testes at developmental stages, we further conducted a preliminary exploration and validation of the O-glycosylation patterns in purified round and elongated spermatids. Using FACS-based DNA ploidy analysis and cell imaging technology, we successfully isolated round spermatids from early developmental mice (day 24, $n = 20$) (Fig. 5a, c) and both round and elongated spermatids from mature developmental mice (week 12, $n = 10$) (Fig. 5b, d). The results of VVA blot and PNA blot suggested that the O-glycosylation profiles of round spermatids from day 24 and week 12 were similar, while the O-glycosylation patterns of elongated spermatids were different from those of round spermatids (Fig. 5e–g). In detail, VVA blot results revealed that the Tn antigen signals at the 50-70 KD protein bands in 12-week-old elongated spermatids were significantly stronger than those in 24-day-old round spermatids (Fig. 5e). This observation partially aligns with mass spectrometry quantification finding that, compared to 24-day-old testes, many up-regulated O-glycoproteins with the highest intensity in 12-week-old testicular tissues (e.g., MENT, NUB1, ACR, and ACRBP) also exhibited molecular weights within the 50–70 kDa range (Fig. 5h). Similarly, reductions in T antigen signals across different molecular weight ranges were observed in both 12-week-old elongated spermatids (Fig. 5f) and 12-week-old testicular tissues (Fig. 5i). These results suggest that the O-glycosylation changes detected by mass spectrometry from 24-day and 12-week-old testicular tissues may primarily originate from the elongated spermatid population.

https://doi.org/10.1038/s41467-025-57980-7

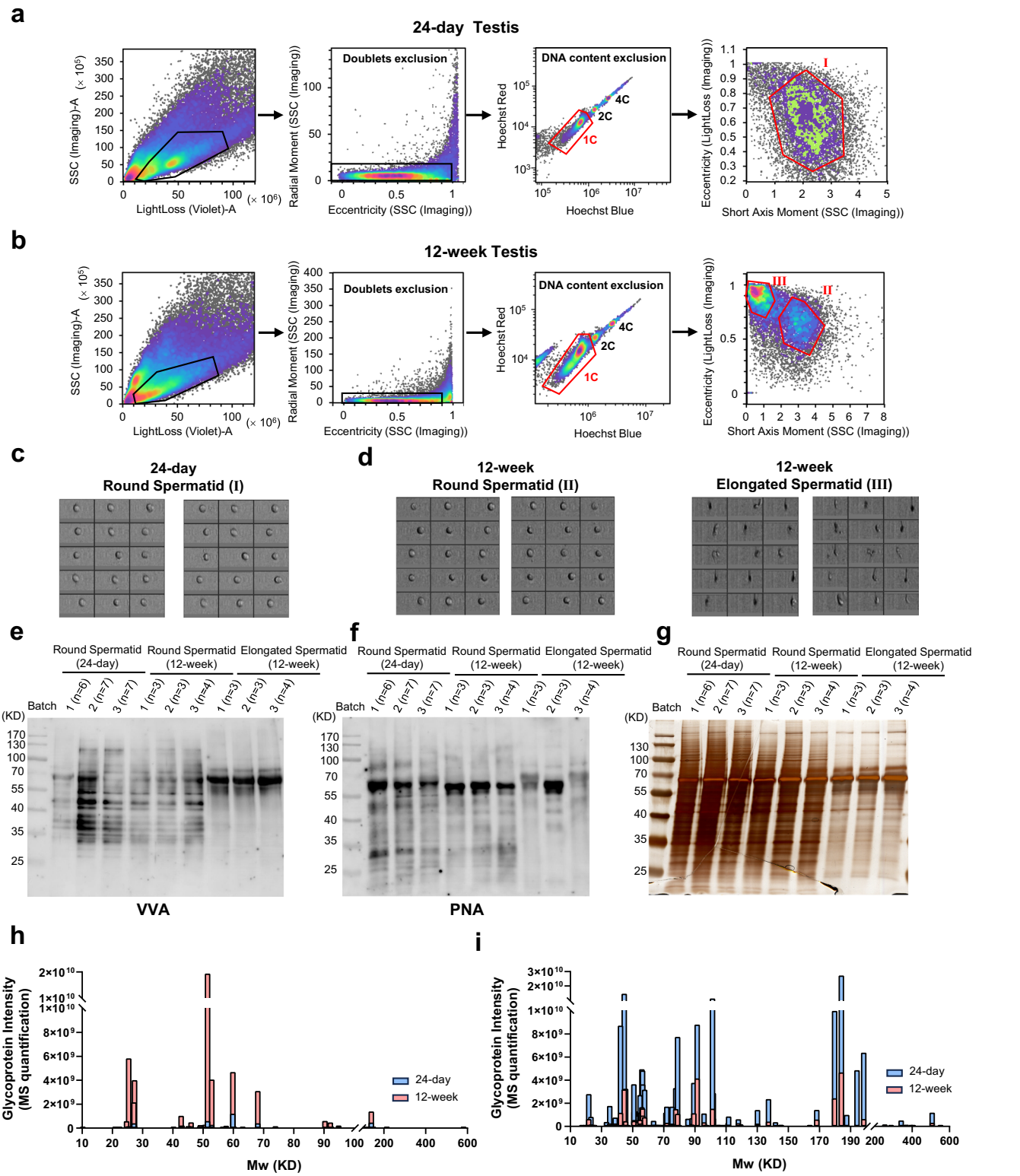

Fig. 5 | O-glycosylation patterns of round and elongated spermatids from 24-day and 12-week testes. a–d Schematic representation of the flow cytometry gating strategy used to sort haploid spermatids from 24-day-old (**a**) and 12-week-old testes (**c**). Cell debris and doublets were first excluded. Subsequently, Hoechst-stained cells were visualized on a Hoechst-blue/Hoechst-red contour plot, and haploid cells with 1C DNA content were gated. The round and elongated spermatids were further distinguished using two imaging parameters (eccentricity and short axis moment). The sorted round spermatids from 24-day testes (**b**), as well as round and elongated spermatids from 12-week testes (**d**), were visualized by BD CellView™ imaging. **e–g** VVA blot (**e**), PNAblot (**f**), and silver staining (**g**) of sorted round and elongated spermatids proteins from 24-day-old ($n = 20$) and 12-week-old ($n = 10$) mice. The number of mice used in each batch was shown. **h**, **i** Molecular weight (Mw) distributions of up-regulated glycoproteins in the VVA-enriched subset (**h**) and down-regulated glycoproteins in the PNA-enriched subset (**i**) in 12-week-old testicular tissues identified by mass spectrometry (MS). The Mw value shown in (**h**, **i**) represents the theoretical molecular weight of the protein plus the molecular weight of the O-glycans identified in this study. VVA *vicia villosa* agglutinin, PNA *peanut* agglutinin. Source data are provided as a Source Data file.

O-glycosylation Affects Interaction between pro-ACR and ACRBP

Finally, we investigated the possible functions of O-glycosylation on testicular proteins. Among the differential proteins associated with spermatogenesis and fertilization, ACR is reported as the major protease of mammalian spermatozoa and plays an indispensable role in sperm penetration of the zona pellucida, with its knockout male mice exhibiting sterile[63,64]. ACR is synthesized and stored in the acrosome as a precursor peptide (pro-ACR), and activated by sequential shearing of C-terminal fragments. ACRBP is the protein that binds to pro-ACR and prevents it from being activated prematurely before the acrosome reaction, with its knockout mice showing severely reduced fertility[65]. It has been reported that ACRBP has two binding domains, B1 and B2, which bind to the SIII and SI domain at the C-terminus of pro-ACR, respectively[66].

In this study, we found that both pro-ACR and ACRBP were highly O-glycosylated, with nine unambiguous O-glycosites on five O-glycopeptides of pro-ACR (Fig. 6a–c) and 16 unambiguous O-glycosites on seven O-glycopeptides of ACRBP (Fig. 6a, b, d). Notably, an increase of O-glycosites for both proteins was found in 12-week-old testis, many of which were located on the binding regions of pro-ACR and ACRBP (Fig. 6a). To further verify whether O-glycosylation affects the interaction between pro-ACR and ACRBP, we overexpressed Flag-tagged pro-ACR and His-tagged ACRBP in CHO and CHO-ldlD cells. The CHO-ldlD cell line is an O-GalNAc glycosylation-deficient cell line due to the mutation in the epimerase that converts UDP-Glc/GlcNAc to UDP-Gal/GalNAc[67]. The results of VVA blot confirmed the absence of O-GalNAc glycosylation on both pro-ACR and ACRBP expressed in CHO-ldlD cells (Fig. 6e). Moreover, co-immunoprecipitation analysis showed that the interaction between ACRBP and pro-ACR was attenuated when O-glycosylation was absent (Fig. 6f), suggesting that O-glycosylation may regulate the functions of pro-ACR and ACRBP by influencing their interaction.

To further explore what glycosyltransferases catalyze O-glycosylation on pro-ACR and ACRBP, we performed in vitro enzyme activity assays using six synthetic peptides targeting the main glycosylation regions of these two proteins (Fig. 6a). Using a published single-cell RNA-seq dataset of mouse testes[68], we found that *Galntl5* and *Galnt3* were the predominant members of ppGalNAc-Ts highly expressed in haploid spermatids, while *Galnt1* was the most highly expressed member in Sertoli cells (Supplementary Fig. 7). The results showed that GALNT3 exhibited stronger catalytic activities than GALNT1, as evidenced by its ability to glycosylate four of the six peptides within a 4 h reaction (Fig. 6g). Notably, two peptides localized in the region where pro-ACR interacts with ACRBP (pro-ACR ① and ③) could be glycosylated by GALNT3 on Thr382, Thr421, and Ser426 (Supplementary Fig. 8). Although GALNTL5 showed remarkably higher expression in round and elongated spermatids, it has no glycosyltransferase activity toward pro-ACR or ACRBP (Fig. 6g), consistent with previous in vitro results using other peptides[20]. Additionally, we tested whether *Galnt7* and *Galnt10* contribute to O-glycosylation of pro-ACR and ACRBP, as these two enzymes were moderately expressed in spermatids. As shown in Supplementary Fig. 9, neither GALNT7 nor GALNT10 exhibited enzyme activity on all naked peptides of pro-ACR and ACRBP. However, when using GALNT3-catalyzed glycopeptides as substrates, both GALNT7 and GALNT10 showed catalytic activities toward glycopeptides of pro-ACR①, pro-ACR③, and ACRBP①, consistent with previous studies indicating that GALNT7 and GALNT10 are strict glycopeptide-preferring isoenzymes[69]. Taken together, these results suggest that GALNT3 may be the major glycosyltransferase responsible for O-glycosylation on pro-ACR and ACRBP, while GALNT7 and GALNT10 may further catalyze these proteins following initial catalysis by GALNT3.

O-glycosylation functions on SPACA7, INSL6, EQTN, and SPESP1

Apart from ACR and ACRBP, we also explored the potential functions of O-glycosylation on four additional highly glycosylated proteins involved in fertilization, i.e., SPACA7, INSL6, EQTN, and SPESP1 (Fig. 4f, g). First, VVA blot results confirmed that the four proteins expressed in CHO-ldlD cells indeed lack O-GalNAc glycosylation (Fig. 7a, c, e, g). Moreover, we found that for all four proteins, a decrease in O-glycosylation corresponded to a decrease in protein stability (Fig. 7b and Supplementary Fig. 10), suggesting that maintaining protein stability may be a fundamental and universal function of O-glycosylation on testicular proteins. Furthermore, we found that O-glycosylation has a variety of other functions. In detail, INSL6 is a secreted protein that undergoes cleavage processing from preproprotein (pro-INSL6) to mature protein[70]. In this study, all eight unambiguous O-glycosites identified were located at its precursor peptide (Supplementary Figs. 11b and 12b). It was also observed that when O-glycosylation was absent, the maturation process of INSL6 was hindered in CHO-ldlD cells, as evidenced by a reduction in the secretion of cleaved peptides (Fig. 7d). EQTN is a type I transmembrane protein widely distributed in the acrosome membrane of mammalian spermatid[71], with 12 unambiguous O-glycosites identified in this study (Supplementary Figs. 11c and 12c). It has been reported that EQTN could interact with SNAP25, a core component of the SNARE complex, during the acrosome reaction[72]. The co-immunoprecipitation analysis showed that the interaction between EQTN and SNAP25 was greatly reduced when O-glycosylation was decreased (Fig. 7f). SPESP1 is another important equatorial protein that initially appears in the matrix of acrosomal vesicles, with its N-terminal region (amino acids 58–102) involved in oligomerization, membrane insertion, and pore formation[73]. In this study, we found eight of the 15 unambiguous O-glycosites on SPESP1 were located at the N-terminal region (Supplementary Figs. 11d and 12d). The results showed that the inhibition of O-glycosylation in CHO-ldlD cells significantly affects the dimerization of SPESP1 (Fig. 7h). Taken together, these results indicate that O-glycosylation on testicular proteins may ultimately affect acrosome formation and acrosome reaction by maintaining protein stability and aggregate structures, as well as promoting protein maturation and protein interactions.

Discussion

Among mammalian organs, the testis is very unique and enigmatic, with the highest number of tissue-enriched expressed proteins (https://www.proteinatlas.org/humanproteome/tissue) and the highest level of O-glycosylation[17]. While the literature has documented the possible role of protein O-glycosylation in male infertility[19,20], the spatial distribution and diversity of O-glycoproteome and temporal dynamics during spermatogenesis remain unmapped.

In this study, we took advantage of advances in lectin enrichment and high-resolution MS with HCD-pd-EThcD, identifying a total of 647 unique O-glycopeptides containing 799 unambiguous O-glycosites from 349 O-glycoproteins and detected 16,227 GPSM, representing the most comprehensive O-glycoproteome map in testis to date. Recently, Yang et al. identified a total of 595 glycoproteins from nine mouse tissues (brain, lung, liver, etc.) and whole blood using EXoO combined with HCD-pd-EThcD MS strategy[35]. Compared to these proteins, we identified 210 O-glycosylated proteins exclusively detected in the testis (Fig. 2e), significantly complementing and expanding the existing mouse tissue O-glycoprotein database. Comparison of identified O-glycoproteins among the 11 organs confirmed that testis is indeed an organ with higher levels of O-glycosylation. In addition, through comparative analysis with previously reported human O-glycoproteins, we were still able to identify an additional 85 O-glycoproteins, including some highly O-glycosylated proteins associated with spermatogenesis (Fig. 2f and Supplementary Data 1). These findings suggest that testicular O-glycosylation is an important, but long-neglected aspect of O-glycosylation research. Moreover, Luo et al. recently identified a total of 68 O-glycoproteins in human seminal plasma and spermatozoa by combining two fragmentation methods of EThcD-sceHCD and sceHCD[58], with EQTN also identified in our study. Despite differences in species, sample sources, and mass spectrometry detection methods, the O-glycosites of EQTN identified in mouse testes and human sperm were

https://doi.org/10.1038/s41467-025-57980-7

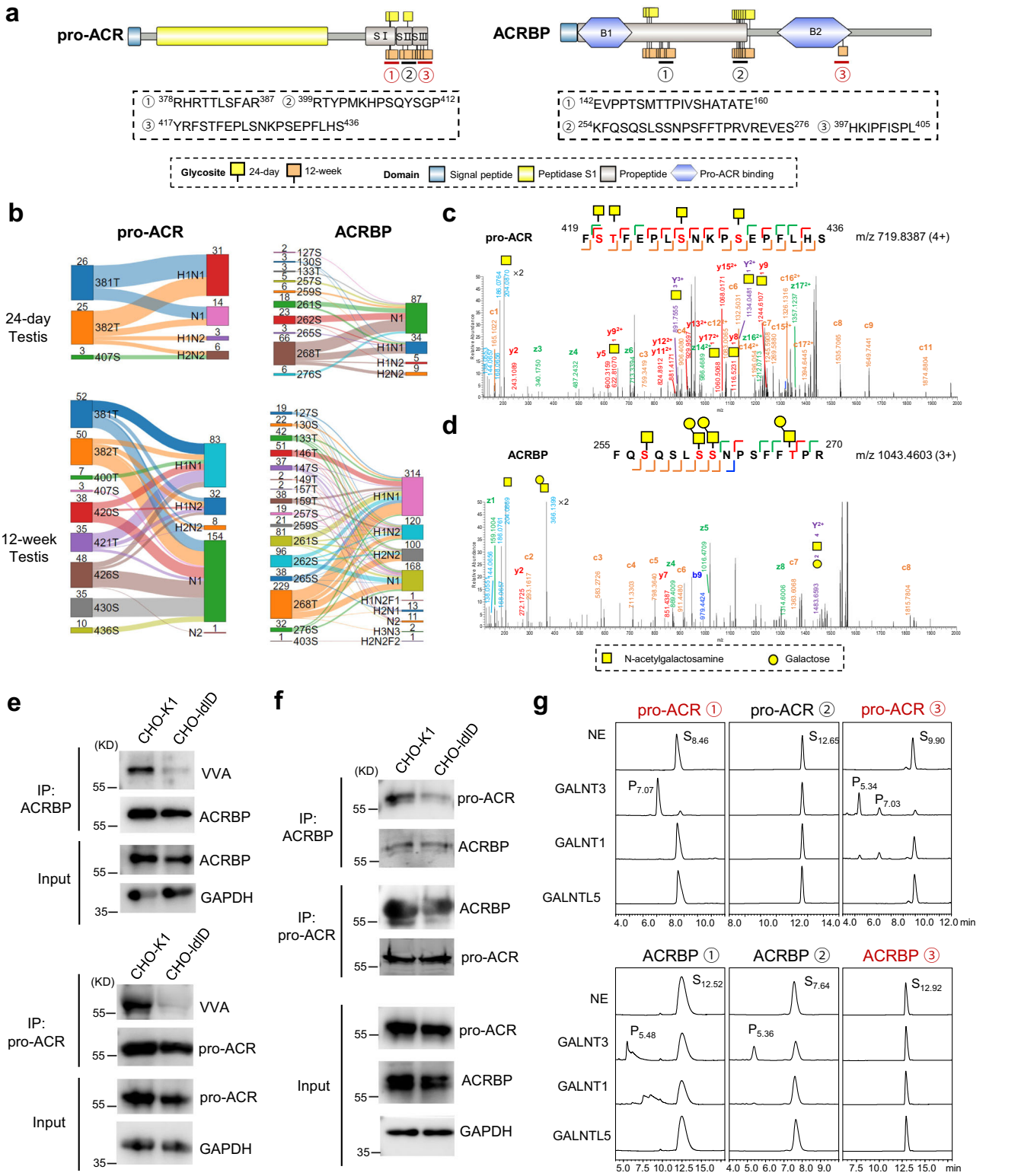

Fig. 6 | O-glycosylation affects interaction of pro-ACR and ACRBP. a Protein schematic representation illustrating the location of O-glycosites on pro-ACR and ACRBP. The schematic positions and sequences of six synthetic peptides of pro-ACR and ACRBP were shown. **b** Sankey diagrams showing site-specific O-glycan changes in the testis from 24 days to 12 weeks. The number of glycopeptide-spectrum matches corresponding to each glycan composition was reflected in the thickness of the flow line and the labeled number on the rectangle. **c**, **d** Representative MS2 spectra showing the O-glycosites and O-glycan structures in glycopeptides of pro-ACR (**c**) and ACRBP (**d**). **e** Flag-tagged pro-ACR or His-tagged ACRBP was transfected into CHO-K1 or CHO-ldlD cells. The VVA signal showing decreased levels of O-GalNAc glycan on proteins expressed in CHO-ldlD cells. **f** Co-Immunoprecipitation analysis of pro-ACR and ACRBP. Flag-tagged pro-ACR and His-tagged ACRBP were co-transfected into CHO-K1 or CHO-ldlD cells. Anti-Flag or anti-His antibody was used to detect the expression of pro-ACR or ACRBP. GAPDH was used as a loading control. **g** Chromatograms of glycosylated products of pro-ACR and ACRBP peptides catalyzed by O-glycosyltransferases GALNT3, GALNT1, and GALNTL5, respectively. The peptides localized in the region where pro-ACR interacts with ACRBP were labeled red. Data in (**e**, **f**) are representative of two or three independent experiments. H Hexose, N N-acetylhexosamine, F Fucose, VVA *vicia villosa* agglutinin. Source data are provided as a Source Data file.

https://doi.org/10.1038/s41467-025-57980-7

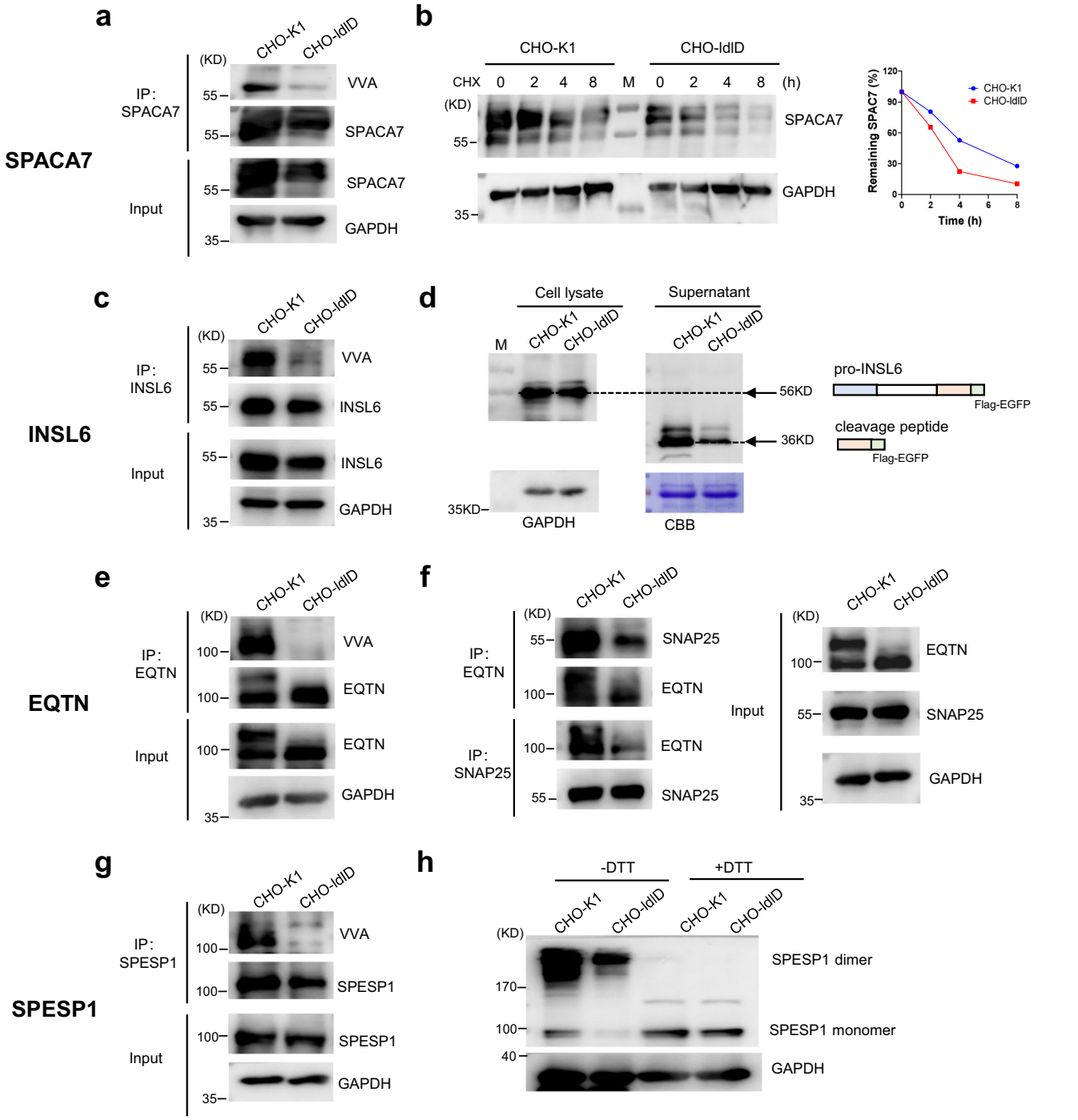

Fig. 7 | O-glycosylation functions on SPACA7, INSL6, EQTN, and SPESP1. The Flag-EGFP-tagged SPACA7 (**a**), INSL6 (**c**), EQTN (**e**), and SPESP1 (**g**) were transfected into CHO-K1 or CHO-IdlD cells. The VVA signals showing decreased levels of O-GalNAc glycan on proteins expressed in CHO-IdlD cells. (**b**) The role of O-glycosylation in protein stability was assessed. CHO cells were treated with 100 μg/mL CHX, and cell lysates were collected at various time points. The intensity of SPACA7 was normalized to that of GAPDH, and the percentage of remaining SPACA7 at different time points was calculated. **d** The role of O-glycosylation in protein maturation and cleavage was evaluated. The cell lysate and culture supernatant from the same batch of CHO cells were collected. The expression of pro-INSL6 and cleavage peptides were detected using anti-Flag antibody. **f** The role of O-glycosylation in protein-protein interaction was investigated. Co-Immunoprecipitation analysis was performed for EQTN and SNAP25. Flag-EGFP-tagged EQTN and His-EGFP-tagged SNAP25 were co-transfected into CHO-K1 or CHO-IdlD cells. Anti-Flag or anti-His antibody was used to detect the expression of EQTN or SNAP25. **h** The role of O-glycosylation in protein dimer formation was examined. Western blot analysis of cell lysates from the CHO cells transfected with SPESP1 under non-denatured or denatured conditions was detected by anti-Flag antibody. Data in (**a**–**h**) are representative of two or three independent experiments. VVA *vicia villosa* agglutinin, CHX cycloheximide, M marker, CBB Coomassie Brilliant Blue stain. Source data are provided as a Source Data file.

mainly located in a similar domain (from amino acids 82–122), and 5 of the 12 O-glycosites we identified were also found in human sperm.

Since the positions of O-glycosites on proteins are closely related to their potential functions, global mapping of the distribution of O-glycosites has gained increasing attention and has been reported in diverse biological models, including genetic engineering cells[36,38], hemostatic system (plasma, platelets, and endothelial cells)[42], and keratinocyte cell lines[48]. In the present study, we assessed whether the

O-glycosites identified in testes were enriched around specific protein structural features based on the annotation in the UniProt database. Our results showed that O-glycosites in testes tended to appear at the outer edges of specific domains, near stem regions and protein cleavage sites, as well as on precursor peptides (Figure S2b). This finding is similar to previous reports in the hemostatic system[42] and keratinocytes[48], suggesting that this may be a universal rule of O-glycan distribution. Compared with statistical results in keratinocytes[48], the highest percentage (19.4%) of O-glycosites in testes was located at the domain edges (Fig. 3e), reinforcing the possibility that O-glycosylation may influence spermatogenesis by stabilizing domain folding or by directly participating in domain function. In addition, our results showed that in testes, LDL receptor Class A was the structural domain with the highest number of identified O-glycosites, with dense O-glycosylation distributed at both the inner and outer edges (Fig. 3e and Supplementary Fig. 2a). This domain is mainly found on low-density lipoprotein receptor (LDLR) and different LDLR-related proteins (LRPs). In this study, we identified LRP1, LRP2, LRP8, LDLR, and VLDLR. Among them, LRP1 has been reported to be required for early embryonic development[74], while LRP8 regulates sperm maturation, and its deficient male mice are sterile[75]. The relatively high abundance of O-glycosylation on LRP1 and LRP8 that we observed may contribute to these functions. Of note, we also identified a structural domain susceptible to O-glycosylation, i.e., the peptidase S1 domain (Fig. 3f). The protease members PRSS40, PRSS42, PRSS43, PRSS44, and PRSS50, which are specifically expressed in germ cells[76,77], were all identified to have intensive O-glycosites near this domain, suggesting that O-glycosylation may modulate spermatogenesis and fertilization by regulating the substrate shearing processes of these proteases.

Additionally, we found that the testicular O-glycoproteome changes dynamically during spermatogenesis. By lectin staining analysis, we found that O-glycosylation in testes was mainly localized in round and elongated spermatids. The glycoforms were predominantly composed of Tn and T antigens, with the Tn structure mainly present in elongated spermatids whereas the T structure signals were stronger in round spermatids (Fig. 1). This finding is basically consistent with previous report by Mandel et al., who stained human testicular tissues and ejaculated spermatozoa using O-glycan antibodies. Their study revealed that O-glycans were not detected in spermatogonia. In contrast, the T structure was present in spermatocytes, haploid spermatids and ejaculated spermatozoa, while the Tn structure was present only in haploid spermatids and ejaculated spermatozoa[18]. Consistent with the lectin staining results, glycan composition analysis and quantitative O-glycoproteome analysis revealed an increased Tn structure and decreased T structure level in sexually mature 12-week-old testes with more elongated spermatids. Moreover, our detection of O-glycosyltransferase suggests that the observed dynamic change in O-glycosylation are at least partially due to elevated expression of GALNT3 and reduced expression of C1GALT1C1 (Supplementary Fig. 13). Intriguingly, it has been reported that GALNT3 was the only active ppGalNAc-T exclusively expressed in spermatocytes and haploid germ cells[18,21], and the VVA signal in the acrosomal regions of spermatids in *Galnt3*$^{-/-}$ mice was drastically reduced[19]. Tabak et al. demonstrated that GALNT3 exhibits a substrate preference for glycine (Gly) and alanine (Ala) at the +2 position, and for proline (Pro), valine (Val), and tyrosine (Tyr) at the −1 position from glycosites[78]. This finding partly align with the amino acid frequencies at the −1 and +2 positions across the 799 unambiguous O-glycosites identified in this study (Supplementary Fig. 14). Our results, combined with these reports, support the significant role of GALNT3 in the dynamic changes of O-glycosylation during spermatogenesis. In addition, our results also suggest that GALNT7 and GALNT10 may contribute to the O-glycosylation in the testes following the initial catalysis by GALNT3.

Finally, since the protein profile of the testis has become clearer only in recent years, the functions of many testicular proteins remain largely unknown. Our studies on O-glycosylation of proteins in the testis provide another window into investigating their functional mechanisms. For example, ACR is preserved in the acrosome as an enzymatically inactive zymogen (pro-ACR) by binding to ACRBP until acrosome exocytosis[65]. This process is important for maintaining the sperm fertilizing ability, and therefore, deletion of these two genes results in infertility or reduced fertility in mice[63–65]. Previous studies have elucidated specific structural domains mediating the binding between ACRBP and pro-ACR. Our study further demonstrates that this binding is dependent on O-glycans of the proteins (Fig. 6), expanding previous knowledge of the interaction of these two proteins. As another example, SPACA7 is a male germ cell-specific protein localized to the sperm acrosome. Currently, only a few studies suggest that it may promote fertilization through some unknown mechanism[79]. Our study reveals that SPACA7 is a highly O-glycosylated protein, with a total of 346 identified GPSM from eight unique O-glycopeptides containing 12 unambiguous O-glycosites, most of which are only detected in 12-week-old testis (Supplementary Figs. 11a and 12a). We also revealed the O-glycosylation of SPACA7 affects its protein stability. These results will provide insights for investigating the functional mechanism of SPACA7. Notably, through preliminary functional studies of several proteins (Fig. 7), we not only discovered the conventional roles of O-GalNAc glycosylation in maintaining protein stability and regulating protein secretion[14], but also found that it may maintain protein dimerization through some direct or indirect effects. This observation may be highly related to the condensation and packaging of secretory granules during acrosomal biogenesis and deserves further investigation.

While this study represents a significant step forward in understanding O-glycosylation in the testis, several open questions also remain. First, we used testicular tissues from different developmental stages rather than purified cell populations for the O-glycoproteomic analysis. Due to the inherently low abundance of glycopeptides and the ion suppression effects of glycosylated sequences compared to unmodified peptides, enrichment of glycopeptides is typically required in O-glycoproteomic experiments. Therefore, the initial sample amount usually needs to be at the milligram level, making it difficult to analyze O-glycoproteome profiling of specific cell populations derived from tissue samples. Furthermore, despite our advanced mass spectrometry strategy enabling the elucidation of over 80% of GPSM for O-glycosites, challenges remain due to the presence of multiple and densely distributed Ser/Thr sites on O-glycopeptides. Consequently, many sites could not been unambiguously identified, leading to a potential underestimation of the relationship between the O-glycans positioning and their regulatory functionalities. In the future, with the development of enrichment methods, mass spectrometry instruments, and analytical software, conducting more in-depth, refined, and comprehensive O-glycoproteomic studies at the level of specific cell populations or even single cell will be the next milestone.

In summary, O-glycosylation is an abundant and important modification in the testis. We established an in-depth and dynamic O-glycoproteome map of mouse testes, assessed O-glycosite preferences, and used acrosomal proteins as an example to illustrate the possible role of ppGalNAc-T-catalyzed O-glycosylation in testicular protein function. Our findings serve as a data resource and roadmap for future functional studies of site-specific O-glycosylation in sperm development and fertilization, and provide insights for investigating the function of testicular proteins that are currently uncharacterized, which will be beneficial for the development of diagnostic and therapeutic approaches for male infertility.

Methods

Mice and testes tissue collection

All experiments were performed in accordance with guidelines approved by the Institutional Animal Care and Use Committee of

Shanghai Jiao Tong University. C57BL/6 J mice were purchased from Charles River Laboratories (Zhejiang, China) and were housed with free access to water and food in a controlled environment with 12h light-dark cycle, room temperature of 20–25 °C and humidity of 40–70%. Mating cages were monitored each morning to determine the exact date of birth, defined as day 0 postnatal. Male mice were euthanized by carbon dioxide inhalation and cervical dislocation, and testes were immediately harvested. For lectin staining, testes were dissected at different postnatal days (on 0, 7, 16, 24 days and 8, 12 weeks, $n = 5$ per group), then fixed with 4% paraformaldehyde. For O-glycoproteomic analysis and Western blotting, testes were collected on postnatal day 24 and week 12 ($n = 4$ per group). For flow cytometry analysis, testes were collected from 24-day-old ($n = 20$) and 12-week-old mice ($n = 10$).

Cell lines, cell culture and transfection

The Chinese hamster ovary epithelial cells CHO-K1 (RRID: CVCL_0214) and its mutant cells CHO-ldlD (RRID: CVCL_1V03) were gifts from Prof. Tatsuro Irimura (The University of Tokyo and Juntendo University School of Medicine, Japan). Both cell lines were maintained in Dulbecco's Modified Eagle Medium/Ham's F-12 (DMEM/F12) 1:1 medium containing 10% FBS and cultured in a humidified atmosphere containing 5% CO_2 at 37 °C.

Plasmids containing Flag-tagged pro-ACR, Flag-EGFP-tagged SPACA7/INSL6/EQTN/ SPESP1, His-tagged ACRBP, or His-EGFP-tagged SNAP25 were transfected into CHO-K1 or CHO-ldlD cells using EZ Trans Transfection Reagent (AC04L091, Life-iLab, Shanghai, China) according to the manufacturer's instructions.

Flow cytometry sorting of spermatids

The testes were surgically removed, and the tunica albuginea along with the remaining blood vessels were removed. After being washed twice in phosphate-buffered saline (PBS), the testes were minced into small fragments using surgical scissors and repeatedly pipetted for 1 min. The suspension was placed at room temperature (RT) for 15 min to enable the precipitation of the remaining large fragments of intact tubules. The supernatant was centrifuged at 700 × g for 10 min, and the pellet was resuspended in 1 mL PBS. Subsequently, the cell suspension was transferred to a FACS tube and stained with 20 μg/mL of Hoechst 33342 (364-07951; Dojindo, Tokyo, Japan) for 30 min at room temperature. The haploid spermatids were gated on Hoechst blue (UV5) and Hoechst red (UV16) channels, and the round and elongated spermatids were distinguished by two imaging parameters (eccentricity and short axis moment) using BD FACSDiscover™ S8 (BD Biosciences, San Jose, CA, USA). The sorted spermatids were visualized by BD CellView™ imaging, and data analysis was performed with BD FACSChorus™ software.

H&E staining and lectin staining

Formalin-fixed, paraffin-embedded (FFPE) testicular sections (5 μm thickness) were deparaffinized and dehydrated. The sections were subjected to Hematoxylin and Eosin (H&E) staining for histological examination. For lectin staining, the sections were transferred to Citrate Antigen Retrieval Solution (P0081; Beyotime, Shanghai, China) to expose antigen epitopes. After washing with PBS, the sections were incubated with Carbo-Free Blocking Solution (SP-5040; Vector Laboratories, Burlingame, CA, USA) for 30 min at RT in a humidified chamber to reduce background staining. The sections were incubated with 10 μg/mL of fluorescein isothiocyanate (FITC)-conjugated *Vicia villosa* agglutinin (VVA) and *Peanut* agglutinin (PNA) (F-4601 and F-2301; EY Laboratories, San Mateo, CA, USA) at 4 °C overnight in the dark. Finally, the sections were incubated with 20 μg/mL of Hoechst 33342 (364-07951; Dojindo) and mounted with VECTASHIELD® Mounting Medium (H-1000; Vector Laboratories). The slides were visualized on a Nikon NI-U ortho-fluorescence microscope.

Immunoprecipitation and immunoblot

Cells were washed with ice-cold PBS and lysed using lysis buffer (150 mM NaCl, 50 mM Tris-HCl, 1 mM EDTA, 0.5% NP-40, pH 7.4) containing protease inhibitor cocktail (04693132001; Roche, Mannheim, Germany). Cell lysate (1 mg) was incubated with 30 μL anti-Flag Affinity Beads (SA042005; Smart-Lifesciences, Shanghai, China) or Ni-NTA Beads 6FF (SA005100; Smart-Lifesciences) overnight at 4 °C with gentle rotation. After washing three times with TBS, the immunoprecipitates were eluted with 20 μL TBS containing 0.2% SDS at 95 °C for 5 min and then centrifuged. The resuspended proteins were subjected to lectin blot or Western blot analysis.

The cell immunoprecipitates, testicular tissue or spermatid cell lysates were separated by SDS-PAGE, transferred to nitrocellulose membranes, and probed with the appropriate antibodies at 4 °C overnight, or with horseradish peroxidase-conjugated VVA/PNA (HRP-VVA/PNA) (1:1000, H-4601/H-2013; EY Laboratories) at room temperature for 2 h. Primary antibodies included anti-Flag antibody (1:1000, M20008L; Abmart, Shanghai, China), anti-His antibody (1:1000, M30111M; Abmart), anti-GALNT3 antibody (1:1000, A13985; ABclonal, Wuhan, China), anti-C1GALT1 antibody (1:1000, A12865; ABclonal), anti-C1GALT1C1 antibody (1:1000, A7590; ABclonal), and anti-GAPDH antibody (1:2000, 10494-1-AP; Proteintech, Rosemont, IL, USA). Immunoreactive bands were visualized using the Amersham ImageQuant 800 ECL imaging system (GE Healthcare, Buckinghamshire, UK) or Odyssey Infrared Imaging System (Li-COR, Lincoln, NE, USA). Total intensities were semi-quantified with Quantity One software (Bio-Rad, Hercules, CA, USA).

HPLC-based GALNTs activity assay

The enzyme activity assay used six naked peptides of pro-ACR and ACRBP (SynPeptide Co., Ltd., Nanjing, China) as substrates. The reaction mixture contained the following components in a final volume of 10 μL: 100 ng of GALNTs in Tris-HCl (25 mM, pH 7.4), 100 μM peptides, 2 mM UDP-GalNAc, and 10 mM MnCl2. The mixture was incubated at 37 °C for 4 h, and then boiled at 95 °C for 5 min to terminate the reaction. The products were separated and detected by reverse-phase HPLC (Shimadzu, Kyoto, Japan) using a C18 analytical column (COSMOSIL 5C18-AR-II, 4.6 × 250 mm) with a flow rate of 1 mL/min.

Glycoproteome analysis

Samples pretreatment. Frozen 24-day or 12-week testes (~100 mg) were resuspended in 500 μL of 50 mM NH_4NO_3 containing 0.1% RapiGest SF (186001861; Waters Corporation) and homogenized using a mortar grinder at 60 Hz for 60 s, repeated three times. The tissue lysates were centrifuged at 150,000 × g at 4 °C for 15 min, and the supernatant was collected for protein quantitation using Pierce BCA protein assay kit (23225; Thermo Fischer Scientific, Waltham, MA, USA). The extracted proteins were heated for 10 min at 80 °C, followed by reduction with 5 mM dithiothreitol (DTT, D0632; MilliporeSigma, St. Louis, MO, USA) at 60 °C for 45 min and alkylation with 10 mM iodoacetamide (IAA, V900335; MilliporeSigma) at RT for 30 min in the dark. Proteins were then digested with trypsin (P01001; Enzyme Zhiyuan Biotechnology, Beijing, China) at a 1:50 wt/wt ratio at 37 °C overnight. The enzyme reaction was terminated by adding trifluoracetic acid (TFA, 302031; MilliporeSigma) and incubating at 37 °C for 20 min. After desalting using a C18 Sep-Pak (WAT054955; Waters Corporation), the sample was treated with 100 U of neuraminidase (N2876; MilliporeSigma) at 37 °C for 2 h.

O-glycopeptides enrichment. Pretreated samples from 24-day or 12-week testes were dissolved in 1 mL binding buffer (VVA-binding buffer: 20 mM Tris-HCl pH 7.4, 150 mM NaCl, 1 mM $CaCl_2$/$MgCl_2$/$MnCl_2$/$ZnCl_2$, and 1 M urea; PNA-binding buffer: 10 mM HEPES pH 7.4, 150 mM NaCl, 1 mM $CaCl_2$, 0.1 mM $MnCl_2$, and 0.1 mM $ZnCl_2$). Then, 100 μL VVA or PNA agarose beads (AL-1233 and AL-1073; Vector Laboratories) were

washed with binding buffer and added to the sample with gentle rotation at 4 °C overnight. After being centrifuged at 800 × g for 3 min, samples were resuspended in 1 mL wash buffer (VVA-washing buffer: binding buffer with 0.4 M glucose; PNA-washing buffer: same as binding buffer) at 4 °C for 5 min to remove the non-specific binding. Finally, the agarose beads were eluted with 100 µL of 0.2 M GalNAc (G0750; MilliporeSigma) for VVA-enriched glycopeptides or 0.5 M galactose (A113374; Aladdin, Shanghai, China) for PNA-enriched glycopeptides with rotation at 4 °C overnight. The eluted of O-glycopeptides were collected and desalted using C18 Spin Tips (84850; Thermo Fischer Scientific) for LC-MS/MS analysis. Each group included four biological replicates.

LC-MS/MS. The enriched glycopeptide fractions were analyzed using an Orbitrap Fusion mass spectrometer (Thermo Fisher Scientific) coupled to a Dionex Ultimate 3000 nanoLC system (Thermo Fisher Scientific). The nanoLC system was operated using an analytical column (Dikma Inspire C18, 3 µm, Canada, 150 mm × 75 µm, self-packed). All samples were dissolved in Buffer A (0.1% formic acid, FA) were injected onto the column and separated using a 120-min gradient from 2% to 5% Buffer B (0.1% formic acid in 100% acetonitrile) in 2 min, from 5% to 20% in 95 min, from 20% to 30% in 10 min and from 30% to 100% in 1 min followed by isocratic elution at 100% for 12 min at a flow rate of 300 nL/min. MS1 scans were acquired with the following settings: scan range, 350–1800 m/z; resolution, 120,000; AGC target, 400,000; maximum injection time, 75 ms; dynamic exclusion time, 60 s. For MS2 scans, precursors with charge states 2–7 were fragmented with higher-energy collisional dissociation (HCD) and electron transfer dissociation (ETD). In HCD scans, collision energy, 28%; resolution, 30,000; maximum injection time, 100 ms; AGC target, 100,000. A subsequent ETD scan of the same precursor was triggered if two of the top 20 most abundant ions in the HCD-MS2 spectrum were included in the following m/z: 126.0550, 138.0549, 144.0655, 168.0654, 186.0760, 204.0865, 274.0921, 292.1027, 290.0870, 308.0976, 366.1395. In ETD scans, resolution, 30,000; AGC target, 100,000; maximum injection time, 150 ms; using the charge-dependent ETD parameters, with 25% supplemental activation.

Glycopeptide identification and quantification. Raw files of LC-MS/MS were identified and quantified using pGlyco3.0[31] and MetaMorpheus (v1.0.2)[32]. The search parameters were as follows: the mass tolerance of the precursor was set to 10 ppm and that of the fragment ion was to 0.02 Da; maximum missed cleavages allowed was two with full specificity; carbamidomethylation of cysteine (Cys) residues was the fixed modification, while methionine (Met) oxidation and protein N-terminal acetylation were variable modifications; the false discovery rate (FDR) was set to 1%. A mouse-specific database (UniProt, Aug. 2023, containing 17,174 reviewed proteins) was the reference proteome.

Moreover, the analysis results derived from pGlyco3.0 were used for label free quantitation by pGlycoQuant (v202302)[80] with the same parameters. Match Between Run (MBR) function in a ± 4 min retention time window was applied and the false quantitation rate (FQR) of the quantitation results was set to 1%. Peptides that had not been quantified in duplicate were excluded.

Bioinformatic annotation and analysis

Protein annotations (domain, cleavage site, etc.) were retrieved from UniProt database and further data analysis was performed by Python (v3.9.13) with in-house scripts and visualized by IBS2.0[81] website (https://ibs.renlab.org/). The Venn diagrams, upset diagrams, heatmaps and volcano plots were made by Hiplot Pro (https://hiplot.com.cn/). PCA, correlation analysis, functional enrichment analysis and sankey diagram were conducted by in-house R (v4.3.1) using factoextra (v1.0.7), corrplot (v0.92), clusterProfiler (v4.8.2), sankeyD3 (v0.3.2) and ggplot2 (v3.4.2) packages. The glycoprotein interaction network was analyzed by STRING database (v11.5) (https://cn.string-db.org/) and visualized by Cytoscape (v3.8.1).

Interrogation of available single-cell transcriptome resources

The single-cell transcriptome data of mouse testes was downloaded from GEO database (GSE121904), processed on the 10X Genomics Chromium System. Data quality control, normalization, and cell clustering were conducted by Seurat (v4.3.0.1) R package. Cell types were manually annotated by marker genes[82].

Statistical analysis

All statistical tests used biological replicates and are indicated by group size (n) in figure legends. Data were expressed as mean ± SEM (standard error of the mean). Statistical analysis was conducted using GraphPad Prism (v8.3.0). Significance was calculated using unpair two-tailed Student's t test or one-tailed Fisher's exact test.

Reporting summary

Further information on research design is available in the Nature Portfolio Reporting Summary linked to this article.

Data availability

The mass spectrometry proteomics data generated in this study have been deposited to the ProteomeXchange Consortium via the iProX partner repository with the dataset identifier PXD047982. The single-cell transcriptome data of mouse testes were extracted from the GEO database GSE121904. The raw data for charts and graphs are provided in the Source Data file. Source data are provided with this paper.

References

1. Eisenberg, M. L. et al. Male infertility. *Nat. Rev. Dis. Prim.* **9**, 49 (2023).
2. Tatum, M. China's fertility treatment boom. *Lancet* **396**, 1622–1623 (2020).
3. Agarwal, A. et al. Male infertility. *Lancet* **397**, 319–333 (2021).
4. Auger, J. Spermatogenic Cells—Structure. *Encycl. Reprod.* **1**, 53–60 (2018).
5. Tecle, E. & Gagneux, P. Sugar-Coated Sperm: Unraveling the Functions of the Mammalian Sperm Glycocalyx. *Mol. Reprod. Dev.* **82**, 635–650 (2015).
6. Wang, G. G. et al. Mapping of the N-Linked Glycoproteome of Human Spermatozoa. *J. Proteome Res.* **12**, 5750–5759 (2013).
7. Xin, M. X. et al. Precision Glycoproteomics Reveals Distinctive N-Glycosylation in Human Spermatozoa. *Mol. Cell. Proteom.* **21**, 100214 (2022).
8. Villaverde, A. I. S. B., Hetherington, L. & Baker, M. A. Quantitative Glycopeptide Changes in Rat Sperm During Epididymal Transit. *Biol. Reprod.* **94**, 91 (2016).
9. Yang, X. Y. et al. Proteomic analysis of *N*-glycosylation of human seminal plasma. *Proteomics* **15**, 1255–1258 (2015).
10. Saraswat, M. et al. N-Glycoproteomics of Human Seminal Plasma Glycoproteins. *J. Proteome Res.* **15**, 991–1001 (2016).
11. Xin, M. M. et al. Precision Structural Interpretation of Site-Specific N-Glycans in Seminal Plasma. *J. Proteome Res.* **21**, 1664–1674 (2022).
12. Biswas, B., Batista, F., Sundaram, S. & Stanley, P. MGAT1 and Complex N-Glycans Regulate ERK Signaling During Spermatogenesis. *Sci. Rep.* **8**, 2022 (2018).
13. Magalhaes, A., Duarte, H. O. & Reis, C. A. The role of O-glycosylation in human disease. *Mol. Asp. Med.* **79**, 100964 (2021).
14. Wandall, H. H., Nielsen, M. A. I., King-Smith, S., de Haan, N. & Bagdonaite, I. Global functions of O-glycosylation: promises and challenges in O-glycobiology. *FEBS J.* **288**, 7183–7212 (2021).

15. Schjoldager, K. T., Narimatsu, Y., Joshi, H. J. & Clausen, H. Global view of human protein glycosylation pathways and functions. *Nat. Rev. Mol. Cell Biol.* **21**, 729–749 (2020).
16. Cervoni, G. E., Cheng, J. J., Stackhouse, K. A., Heimburg-Molinaro, J. & Cummings, R. D. O-glycan recognition and function in mice and human cancers. *Biochem. J.* **477**, 1541–1564 (2020).
17. Zou, X. et al. A standardized method for lectin microarray-based tissue glycome mapping. *Sci. Rep.* **7**, 43560 (2017).
18. Rajpert-De Meyts, E. et al. Changes in the profile of simple mucin-type O-glycans and polypeptide GalNAc-transferases in human testis and testicular neoplasms are associated with germ cell maturation and tumour differentiation. *Virchows Arch.* **451**, 805–814 (2007).
19. Miyazaki, T. et al. Galnt3 deficiency disrupts acrosome formation and leads to oligoasthenoteratozoospermia. *Histochem. Cell Biol.* **139**, 339–354 (2013).
20. Takasaki, N. et al. A heterozygous mutation of *GALNTL5* affects male infertility with impairment of sperm motility. *Proc. Natl Acad. Sci. USA.* **111**, 1120–1125 (2014).
21. Nygaard, M. B. et al. Expression of the O-Glycosylation Enzyme GalNAc-T3 in the Equatorial Segment Correlates with the Quality of Spermatozoa. *Int. J. Mol. Sci.* **19**, 2949 (2018).
22. Xin, A. J. et al. Lectin binding of human sperm associates with *DEFB126* mutation and serves as a potential biomarker for subfertility. *Sci. Rep.* **6**, 20249 (2016).
23. Nagai-Okatani, C. et al. LM-GlycomeAtlas Ver. 2.0: An Integrated Visualization for Lectin Microarray-based Mouse Tissue Glycome Mapping Data with Lectin Histochemistry. *J. Proteome Res.* **20**, 2069–2075 (2021).
24. Bellvé, A. R. et al. Spermatogenic cells of the prepuberal mouse. Isolation and morphological characterization. *J. Cell Biol.* **74**, 68–85 (1977).
25. Montoto, L. G., Arregui, L., Sanchez, N. M., Gomendio, M. & Roldan, E. R. Postnatal testicular development in mouse species with different levels of sperm competition. *Reproduction* **143**, 333–346 (2012).
26. Borg, C. L., Wolski, K. M., Gibbs, G. M. & O'Bryan, M. K. Phenotyping male infertility in the mouse: how to get the most out of a 'non-performer'. *Hum. Reprod. Update* **16**, 205–224 (2010).
27. Tollefsen, S. E. & Kornfeld, R. Isolation and characterization of lectins from Vicia villosa. Two distinct carbohydrate binding activities are present in seed extracts. *J. Biol. Chem.* **258**, 5165–5171 (1983).
28. Tollefsen, S. E. & Kornfeld, R. The B4 lectin from Vicia villosa seeds interacts with N-acetylgalactosamine residues alpha-linked to serine or threonine residues in cell surface glycoproteins. *J. Biol. Chem.* **258**, 5172–5176 (1983).
29. Puri, K. D., Gopalakrishnan, B. & Surolia, A. Carbohydrate binding specificity of the Tn-antigen binding lectin from Vicia villosa seeds (VVLB4). *FEBS Lett.* **312**, 208–212 (1992).
30. Lotan, R., Skutelsky, E., Danon, D. & Sharon, N. The purification, composition, and specificity of the anti-T lectin from peanut (Arachis hypogaea). *J. Biol. Chem.* **250**, 8518–8523 (1975).
31. Zeng, W. F., Cao, W. Q., Liu, M. Q., He, S. M. & Yang, P. Y. Precise, fast and comprehensive analysis of intact glycopeptides and modified glycans with pGlyco3. *Nat. Methods* **18**, 1515–1523 (2021).
32. Lu, L., Riley, N. M., Shortreed, M. R., Bertozzi, C. R. & Smith, L. M. O-Pair Search with MetaMorpheus for O-glycopeptide characterization. *Nat. Methods* **17**, 1133–1138 (2020).
33. Li, W., Hou, C., Li, Y., Wu, C. & Ma, J. HexNAcQuest: A Tool to Distinguish O-GlcNAc and O-GalNAc. *J. Am. Soc. Mass Spectrom.* **33**, 2008–2012 (2022).
34. Lin, J. B. & Troyer, D. Testicular Anatomy and Physiology. In *Pathobiology of Human Disease* (eds McManus LM, Mitchell RN). (Academic Press, 2014).
35. Yang, W. et al. Quantitative mapping of the in vivo O-GalNAc glycoproteome in mouse tissues identifies GalNAc-T2 O-glycosites in metabolic disorder. *Proc. Natl Acad. Sci. USA.* **120**, e2303703120 (2023).
36. Steentoft, C. et al. Mining the O-glycoproteome using zinc-finger nuclease-glycoengineered SimpleCell lines. *Nat. Methods* **8**, 977–982 (2011).
37. Schjoldager, K. T. et al. Probing isoform-specific functions of polypeptide GalNAc-transferases using zinc finger nuclease glycoengineered SimpleCells. *Proc. Natl Acad. Sci. USA.* **109**, 9893–9898 (2012).
38. Steentoft, C. et al. Precision mapping of the human O-GalNAc glycoproteome through SimpleCell technology. *EMBO J.* **32**, 1478–1488 (2013).
39. Vakhrushev, S. Y. et al. Enhanced mass spectrometric mapping of the human GalNAc-type O-glycoproteome with SimpleCells. *Mol. Cell. Proteom.* **12**, 932–944 (2013).
40. Campos, D. et al. Probing the O-glycoproteome of gastric cancer cell lines for biomarker discovery. *Mol. Cell. Proteom.* **14**, 1616–1629 (2015).
41. Schjoldager, K. T. et al. Deconstruction of O-glycosylation–GalNAc-T isoforms direct distinct subsets of the O-glycoproteome. *EMBO Rep.* **16**, 1713–1722 (2015).
42. King, S. L. et al. Characterizing the O-glycosylation landscape of human plasma, platelets, and endothelial cells. *Blood Adv.* **1**, 429–442 (2017).
43. Goth, C. K., Vakhrushev, S. Y., Joshi, H. J., Clausen, H. & Schjoldager, K. T. Fine-Tuning Limited Proteolysis: A Major Role for Regulated Site-Specific O-Glycosylation. *Trends Biochem. Sci.* **43**, 269–284 (2018).
44. Hintze, J. et al. Probing the contribution of individual polypeptide GalNAc-transferase isoforms to the O-glycoproteome by inducible expression in isogenic cell lines. *J. Biol. Chem.* **293**, 19064–19077 (2018).
45. Wang, S. et al. Site-specific O-glycosylation of members of the low-density lipoprotein receptor superfamily enhances ligand interactions. *J. Biol. Chem.* **293**, 7408–7422 (2018).
46. Narimatsu, Y. et al. Exploring Regulation of Protein O-Glycosylation in Isogenic Human HEK293 Cells by Differential O-Glycoproteomics. *Mol. Cell. Proteom.* **18**, 1396–1409 (2019).
47. Madsen, T. D. et al. An atlas of O-linked glycosylation on peptide hormones reveals diverse biological roles. *Nat. Commun.* **11**, 4033 (2020).
48. Nielsen, M. I. et al. Global mapping of GalNAc-T isoform-specificities and O-glycosylation site-occupancy in a tissue-forming human cell line. *Nat. Commun.* **13**, 6257 (2022).
49. Pap, A., Kiraly, I. E., Medzihradszky, K. F. & Darula, Z. Multiple Layers of Complexity in O-Glycosylation Illustrated With the Urinary Glycoproteome. *Mol. Cell. Proteom.* **21**, 100439 (2022).
50. Takakura, D. et al. Targeted O-glycoproteomics for the development of diagnostic markers for advanced colorectal cancer. *Front. Oncol.* **13**, 1104936 (2023).
51. Halim, A., Nilsson, J., Ruetschi, U., Hesse, C. & Larson, G. Human urinary glycoproteomics; attachment site specific analysis of N- and O-linked glycosylations by CID and ECD. *Mol. Cell. Proteom.* **11**, M111 013649 (2012).
52. Halim, A., Ruetschi, U., Larson, G. & Nilsson, J. LC-MS/MS characterization of O-glycosylation sites and glycan structures of human cerebrospinal fluid glycoproteins. *J. Proteome Res.* **12**, 573–584 (2013).
53. Hoffmann, M., Marx, K., Reichl, U., Wuhrer, M. & Rapp, E. Site-specific O-Glycosylation Analysis of Human Blood Plasma Proteins. *Mol. Cell. Proteom.* **15**, 624–641 (2016).

54. Qin, H. et al. Proteomics Analysis of O-GalNAc Glycosylation in Human Serum by an Integrated Strategy. *Anal. Chem.* **89**, 1469–1476 (2017).
55. Zhao, X. et al. An Integrated Mass Spectroscopy Data Processing Strategy for Fast Identification, In-Depth, and Reproducible Quantification of Protein O-Glycosylation in a Large Cohort of Human Urine Samples. *Anal. Chem.* **92**, 690–698 (2020).
56. Yue, X. et al. Highly Efficient Enrichment of O-GalNAc Glycopeptides by Using Immobilized Metal Ion Affinity Chromatography. *Anal. Chem.* **93**, 7579–7587 (2021).
57. Chen, Z. et al. In-Depth Site-Specific O-Glycosylation Analysis of Glycoproteins and Endogenous Peptides in Cerebrospinal Fluid (CSF) from Healthy Individuals, Mild Cognitive Impairment (MCI), and Alzheimer's Disease (AD) Patients. *ACS Chem. Biol.* **17**, 3059–3068 (2022).
58. Luo, M. et al. GlycoTCFM: Glycoproteomics Based on Two Complementary Fragmentation Methods Reveals Distinctive O-Glycosylation in Human Sperm and Seminal Plasma. *J. Proteome Res.* **22**, 3833–3842 (2023).
59. Yang, W., Ao, M., Hu, Y., Li, Q. K. & Zhang, H. Mapping the O-glycoproteome using site-specific extraction of O-linked glycopeptides (EXoO). *Mol. Syst. Biol.* **14**, e8486 (2018).
60. Yang, W. et al. Mass Spectrometric Mapping of Glycoproteins Modified by Tn-Antigen Using Solid-Phase Capture and Enzymatic Release. *Anal. Chem.* **92**, 9230–9238 (2020).
61. Gan, H. et al. Integrative proteomic and transcriptomic analyses reveal multiple post-transcriptional regulatory mechanisms of mouse spermatogenesis. *Mol. Cell Proteom.* **12**, 1144–1157 (2013).
62. Li, M. et al. Comparative proteomic analysis of round and elongated spermatids during spermiogenesis in mice. *Biomed. Chromatogr.* **34**, e4799 (2020).
63. Klemm, U., Müller-Esterl, W. & Engel, W. Acrosin, the peculiar sperm-specific serine protease. *Hum. Genet.* **87**, 635–641 (1991).
64. Hirose, M. et al. Acrosin is essential for sperm penetration through the zona pellucida in hamsters. *Proc. Natl Acad. Sci. USA.* **117**, 2513–2518 (2020).
65. Kanemori, Y. et al. Biogenesis of sperm acrosome is regulated by pre-mRNA alternative splicing of Acrbp in the mouse. *Proc. Natl Acad. Sci. USA.* **113**, E3696–E3705 (2016).
66. Kanemori, Y. et al. Two functional forms of ACRBP/sp32 are produced by pre-mRNA alternative splicing in the mouse. *Biol. Reprod.* **88**, 105 (2013).
67. Kingsley, D. M., Kozarsky, K. F., Hobbie, L. & Krieger, M. Reversible defects in O-linked glycosylation and LDL receptor expression in a UDP-Gal/UDP-GalNAc 4-epimerase deficient mutant. *Cell* **44**, 749–759 (1986).
68. Copenhaver, G. P. et al. Dynamic transcriptome profiles within spermatogonial and spermatocyte populations during postnatal testis maturation revealed by single-cell sequencing. *PLoS Genet.* **15**, e1007810 (2019).
69. de Las Rivas, M., Lira-Navarrete, E., Gerken, T. A. & Hurtado-Guerrero, R. Polypeptide GalNAc-Ts: from redundancy to specificity. *Curr. Opin. Struct. Biol.* **56**, 87–96 (2019).
70. Lu, C. X. et al. Insulin-like peptide 6: Characterization of secretory status and posttranslational modifications. *Endocrinology* **147**, 5611–5623 (2006).
71. Yamatoya, K. et al. Equatorin: identification and characterization of the epitope of the MN9 antibody in the mouse. *Biol. Reprod.* **81**, 889–897 (2009).
72. Hao, J. et al. Equatorin is not essential for acrosome biogenesis but is required for the acrosome reaction. *Biochem Biophys. Res Commun.* **444**, 537–542 (2014).
73. Wolkowicz, M. J. et al. Equatorial segment protein (ESP) is a human alloantigen involved in sperm-egg binding and fusion. *J. Androl.* **29**, 272–282 (2008).
74. Herz, J., Clouthier, D. E. & Hammer, R. E. LDL receptor-related protein internalizes and degrades uPA-PAI-1 complexes and is essential for embryo implantation. *Cell* **71**, 411–421 (1992).
75. Andersen, O. M. et al. Essential role of the apolipoprotein E receptor-2 in sperm development. *J. Biol. Chem.* **278**, 23989–23995 (2003).
76. Kohno, N. et al. Two novel testicular serine proteases, TESP1 and TESP2, are present in the mouse sperm acrosome. *Biochem. Biophys. Res. Commun.* **245**, 658–665 (1998).
77. Yoneda, R. et al. Three testis-specific paralogous serine proteases play different roles in murine spermatogenesis and are involved in germ cell survival during meiosis. *Biol. Reprod.* **88**, 118 (2013).
78. Gerken, T. A. et al. Emerging paradigms for the initiation of mucin-type protein O-glycosylation by the polypeptide GalNAc transferase family of glycosyltransferases. *J. Biol. Chem.* **286**, 14493–14507 (2011).
79. Nguyen, E. B., Westmuckett, A. D. & Moore, K. L. SPACA7 is a novel male germ cell-specific protein localized to the sperm acrosome that is involved in fertilization in mice. *Biol. Reprod.* **90**, 16 (2014).
80. Kong, S. et al. pGlycoQuant with a deep residual network for quantitative glycoproteomics at intact glycopeptide level. *Nat. Commun.* **13**, 7539 (2022).
81. Xie, Y. et al. IBS 2.0: an upgraded illustrator for the visualization of biological sequences. *Nucleic Acids Res.* **50**, W420–W426 (2022).
82. Chen, Y. et al. Single-cell RNA-seq uncovers dynamic processes and critical regulators in mouse spermatogenesis. *Cell Res.* **28**, 879–896 (2018).

Acknowledgements

We thank Yandong An from BD Biosciences for assistance with imaging flow cytometry. This work was supported by National Natural Science Foundation of China (92478203, 32371332, and 32071271 to Y.Z., 32271340 to X.Z.), Shanghai Sailing Program (18YF1410500 to X.Z.), Natural Science Foundation of Shanghai (23ZR1435600 to X.Z.), and Shanghai Pilot Program for Basic Research- Shanghai Jiao Tong University (21TQ1400210 to Y.Z.).

Author contributions

X.Z. and Y.Z. designed research; Q.L., X.L., Y.D., H.Z., and H.L. performed experiments; Q.L., Y.D., R.W., and X.Z. analyzed data; Y.F., J.W., and F.M. gave technical or material support; X.Z. and Y.Z. supervised research; X.Z. and Q.L. wrote the paper; Y.Z. edited the paper.

Competing interests

The authors declare no competing interests.

Additional information

Supplementary information The online version contains supplementary material available at https://doi.org/10.1038/s41467-025-57980-7.

Correspondence and requests for materials should be addressed to Yan Zhang or Xia Zou.

Peer review information *Nature Communications* thanks Hubert Schorle, who co-reviewed with AnđelaKovačevićKristian Almstrup, and Yong Zhang for their contribution to the peer review of this work. A peer review file is available.